



ALMA MATER STUDIORUM  
UNIVERSITÀ DI BOLOGNA

ARCHIVIO ISTITUZIONALE  
DELLA RICERCA

## Alma Mater Studiorum Università di Bologna Archivio istituzionale della ricerca

Characterizing magma fragmentation and its relationship with eruptive styles of Somma-Vesuvius volcano (Naples, Italy)

This is the final peer-reviewed author's accepted manuscript (postprint) of the following publication:

*Published Version:*

Poret, M., Di Donato, M., Costa, A., Sulpizio, R., Mele, D., Lucchi, F. (2020). Characterizing magma fragmentation and its relationship with eruptive styles of Somma-Vesuvius volcano (Naples, Italy). *JOURNAL OF VOLCANOLOGY AND GEOTHERMAL RESEARCH*, 393, 1-17 [10.1016/j.jvolgeores.2019.106683].

*Availability:*

This version is available at: <https://hdl.handle.net/11585/799817> since: 2021-02-16

*Published:*

DOI: <http://doi.org/10.1016/j.jvolgeores.2019.106683>

*Terms of use:*

Some rights reserved. The terms and conditions for the reuse of this version of the manuscript are specified in the publishing policy. For all terms of use and more information see the publisher's website.

This item was downloaded from IRIS Università di Bologna (<https://cris.unibo.it/>).  
When citing, please refer to the published version.

(Article begins on next page)

## Manuscript Details

<b>Manuscript number</b>	VOLGEO_2019_161
<b>Title</b>	Characterizing magma fragmentation and its relationship with eruptive styles of Somma-Vesuvius volcano (Naples, Italy)
<b>Article type</b>	Research Paper

### Abstract

Among the active volcanoes worldwide, Somma-Vesuvius, in Italy, is one with the highest volcanic risk as the surrounding areas are highly populated. Somma-Vesuvius is quiescent since 1944, but geological and historical records revealed a frequent violent explosive activity in the last 4000 years, representing a severe risk for the actual 700000 inhabitants living in the red zone (the area having a high probability for being impacted by pyroclastic density currents) and more than one million people who can be potentially affected by tephra fallout. This study aims at analysing the distribution of tephra fallout deposits and grain-size data from several Somma-Vesuvius eruptions of different styles, ranging from Violent Strombolian to sub-Plinian and Plinian, for characterizing the associated magmatic fragmentation through the assessment of the total grain-size distribution (TGSD). Chronologically, we focus on the Avellino (4365 BP) and Pompeii (A.D. 79) Plinian eruptions, Pollena (A.D. 472) sub-Plinian eruption, and the 1906 and 1944 Violent Strombolian eruptions. The related TGSDs were estimated by means of the Voronoi tessellation method, which, beside a suitable number of local grain-size distributions, requires the delimitation of the minimum tephra loading (zero-line contour). TGSDs for the different eruptive styles are needed by tephra dispersal models for reconstructing or predicting both tephra loading and airborne ash dispersal. However, due to the typical paucity of available field outcrops, field-derived TGSDs can be biased towards the coarse and fine populations. To encompass this issue, we performed a sensitivity study on the assumption behind TGSD reconstruction and described TGSD through analytical distributions, which best fit the field TGSDs. Our main objective is a more robust estimation of the TGSDs associated with the different eruptive styles. Characterizing such TGSDs, and the other eruption source parameters, is crucial for robustly predicting tephra loading and airborne ash dispersal of future eruptions at Somma-Vesuvius.

<b>Keywords</b>	Total grain-size distribution; Bulk granulometry; Eruption source parameters; Tephra fallout; Volcanic hazards assessment
<b>Corresponding Author</b>	Matthieu Poret
<b>Corresponding Author's Institution</b>	Istituto Nazionale di Geofisica e Vulcanologia
<b>Order of Authors</b>	Matthieu Poret, Miriana Di Donato, Antonio Costa, Roberto Sulpizio, Daniela Mele, Federico Lucchi
<b>Suggested reviewers</b>	Daniele Andronico, mauro antonio di vito, Guido Giordano, Bruce Houghton

## Submission Files Included in this PDF

### File Name [File Type]

Cover Letter.pdf [Cover Letter]

Highlights.docx [Highlights]

Poret\_et\_al\_v3.2.docx [Manuscript File]

## Submission Files Not Included in this PDF

### File Name [File Type]

Fig. 1 - Context.png [Figure]

Fig. 2 - GSD - Avellino.png [Figure]

Fig. 3 - GSD - Pollena.png [Figure]

Fig. 4 - GSD - 1906.png [Figure]

Fig. 5 - GSD - 1944.png [Figure]

Fig. 6 - TGSD.png [Figure]

Table S1.xlsx [Table]

Table S2.xlsx [Table]

Table S3.xlsx [Table]

Table S4.xlsx [Table]

To view all the submission files, including those not included in the PDF, click on the manuscript title on your EVISE Homepage, then click 'Download zip file'.

Dr. Matthieu Poret  
Laboratoire Magmas et Volcans  
63000 Clermont-Ferrand  
France  
matthieu.poret@gmail.com

Dear Executive Editor,

Please find enclosed the manuscript entitled “Characterizing magma fragmentation and its relationship with eruptive styles of Somma-Vesuvius volcano (Naples, Italy)” by Matthieu Poret, Miriana Di Donato, Antonio Costa, Roberto Sulpizio, Daniela Mele, and Federico Lucchi to be considered for publication in Journal of Volcanology and Geothermal Research. Our work provides an assessment of the total grain size distributions (TGSD) on the basis of field data analysis for different eruptions of Somma-Vesuvius, helping to characterize magma fragmentation for the different eruptive styles analysed (i.e. from Violent Strombolian to Plinian). We focused on the Avellino and Pompeii Plinian eruptions, the Pollena sub-Plinian eruption, and the 1906 and 1944 Violent Strombolian eruptions.

For achieving this aim, we analysed field-data from the literature together with new data for assessing georeferenced grain size distributions at sites representative of the proximal, medial, and distal areas. By means of this dataset, we estimated the TGSDs for the Avellino, Pollena, 1906, and 1944 eruptions. We also studied the sensitivity of the Voronoi tessellation method used for such reconstructions. Although the number of tephra samples is limited, it covers proximal, medial, and distal areas, providing the current best approximations of the TGSDs relative to each eruption. TGSDs obtained through the Voronoi tessellation method were also estimated by means of analytical distributions (i.e. as sum of i) two lognormal and ii) two Weibull distributions), which allow for extrapolating field TGSDs. By comparing the TGSDs associated with the different eruptive styles, our results indicate that increasing the eruption intensity, i.e. going from Violent Strombolian to Plinian eruptive style, and the efficiency of magma fragmentation also increases. Moreover, they also show the significance of magma-water interaction on the amount of fines of the reconstructed TGSDs.

We hope you will find this study interesting and we believe that our results stimulate further works focussing on better characterizing TGSDs of other volcanic eruptions worldwide. In particular, the estimates of the TGSD for each eruption, representative of Violent Strombolian, sub-Plinian and Plinian styles, can be used as input for numerical models aimed at reconstructing past eruptions or tephra hazard assessment for similar scenarios.

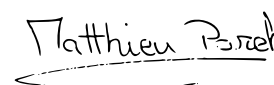
On behalf of all co-authors, we declare no competing financial interests.

We hope that the content of this article will be of a broad interest to the Journal of Volcanology and Geothermal Research.

We are looking forward to your editorial decision.

Yours sincerely,

**Matthieu Poret**

A handwritten signature in black ink that reads "Matthieu Poret". The signature is written in a cursive style and is underlined with a single horizontal line.

## Highlights

- 1 Tephra deposits of 4 different eruptions of Vesuvius were analyzed
- 2 Deposit volumes and bulk granulometries were reconstructed from field data analysis
- 3 Performed comparative study for different eruption and magma fragmentation styles
- 4 Results are important for tephra dispersal modelling and hazard assessment purposes

# Characterizing magma fragmentation and its relationship with eruptive styles of Somma-Vesuvius volcano (Naples, Italy)

Matthieu Poret <sup>1\*</sup>, Miriana Di Donato <sup>2</sup>, Antonio Costa <sup>1</sup>, Roberto Sulpizio <sup>3</sup>,  
Daniela Mele <sup>3</sup>, and Federico Lucchi <sup>2</sup>

<sup>1</sup> Université Clermont Auvergne, CNRS, IRD, OPGC, Laboratoire Magmas et Volcans, Clermont-Ferrand, France

<sup>2</sup> Università di Bologna, Dipartimento di Scienze Biologiche, Geologiche e Ambientali, Bologna, Italy

<sup>3</sup> Università di Bari, Dipartimento di Scienze della Terra e Geoambientali, Bari, Italy

\* Corresponding author e-mail: matthieu.poret@gmail.com

## Abstract

Among the active volcanoes worldwide, Somma-Vesuvius, in Italy, is one with the highest volcanic risk as the surrounding areas are highly populated. Somma-Vesuvius is quiescent since 1944, but geological and historical records revealed a frequent violent explosive activity in the last 4000 years, representing a severe risk for the actual 700000 inhabitants living in the red zone (the area having a high probability for being impacted by pyroclastic density currents) and more than one million people who can be potentially affected by tephra fallout. This study aims at analysing the distribution of tephra fallout deposits and grain-size data from several Somma-Vesuvius eruptions of different styles, ranging from Violent Strombolian to sub-Plinian and Plinian, for characterizing the associated magmatic fragmentation through the assessment of the total grain-size distribution (TGSD). Chronologically, we focus on the Avellino (4365 BP) and Pompeii (A.D. 79) Plinian eruptions, Pollena (A.D. 472) sub-Plinian eruption, and the 1906 and 1944 Violent Strombolian eruptions. The related TGSDs were estimated by means of the Voronoi tessellation method, which, beside a suitable number of local grain-size distributions, requires the delimitation of the minimum tephra loading (zero-line contour). TGSDs for the different eruptive styles are needed by tephra dispersal models for reconstructing or predicting both tephra loading and airborne ash dispersal. However, due to the typical paucity of available field outcrops, field-derived TGSDs can be biased towards the coarse and fine populations. To encompass this issue, we performed a sensitivity study on the assumption behind TGSD reconstruction and described TGSD through analytical distributions, which best fit the field TGSDs. Our main objective is a more robust estimation of the TGSDs associated with the different eruptive styles. Characterizing such TGSDs, and the other eruption source parameters, is crucial for robustly predicting tephra loading and airborne ash dispersal of future eruptions at Somma-Vesuvius.

**Keywords:** Total grain-size distribution; Bulk granulometry; Eruption source parameters; Tephra fallout; Volcanic hazards assessment

## 34 **1 Introduction**

35 The Somma-Vesuvius volcanic complex is one of the most studied volcanoes in the world, and is  
36 included among the highest volcanic risks in the world (e.g. Macedonio et al., 2008). One of the  
37 main goals of modern volcanology is a quantitative assessment of volcanic hazards (e.g. tephra  
38 loading, airborne ash dispersal) in sensitive areas like those surrounding Somma-Vesuvius, where  
39 they can heavily impact the metropolitan city of Naples (Italy) with potential severe consequences  
40 for the central Mediterranean zone (Folch and Sulpizio, 2010; Sulpizio et al., 2014). For a robust  
41 volcanic hazard assessment, we must know the eruptive history of the volcano and its past  
42 behaviour (e.g. Cioni et al., 2008; Santacroce et al., 2008). Such information derives typically from  
43 the analysis of geological records (e.g. Cioni et al., 1999; 2008; Santacroce and Sbrana, 2003;  
44 Santacroce et al., 2008; Gurioli et al., 2010; Sulpizio et al., 2010a; 2010b; 2010c; 2010d; 2014). In  
45 fact, analysis of geological data allows assessing the key eruption source parameters (ESP)  
46 associated with an eruption, such as the total erupted mass (TEM; i.e. eruption magnitude), mass  
47 eruption rate (MER; i.e. eruption intensity), eruptive column height, and total grain-size distribution  
48 (TGSD), which depends on the intensity and behaviour of the initial magma fragmentation  
49 (Bonadonna and Houghton, 2005; Bonadonna et al., 2015; Costa et al., 2016). To investigate the  
50 effect of different magma compositions and eruption intensity on ESPs, we selected four eruptions  
51 from the eruptive record of Somma-Vesuvius, representative of its most frequent eruptive styles. In  
52 particular, we considered the Avellino Plinian eruption (c.a. 3900 years BP; Sevink et al., 2011), the  
53 Pollena sub-Plinian eruption (A.D. 472; Sulpizio et al., 2005; Santacroce et al., 2008; Foch and  
54 Sulpizio, 2010), and the Violent Strombolian eruptions of 1906 (Mercalli, 1906; Arrighi et al.,  
55 2001) and 1944 (Imbò, 1949; Cubellis et al., 2013). Moreover, for comparison purposes, we also  
56 considered the TGSD of the Pompeii Plinian eruption (A.D. 79) derived from Macedonio et al.  
57 (1988; 2008). The literature reports petrochemical and lithological features of the tephra deposits  
58 for these four eruptions (e.g. Imbò, 1949; Macedonio et al., 1988; Arrighi et al., 2001; Cioni et al.,  
59 1999; 2003a; 2003b; 2004; 2008; Sulpizio et al., 2005; 2007; 2008; 2010a; 2010b; 2010c; 2010d;  
60 2012; 2014; Cole and Scarpati, 2010; Cubellis et al., 2013; Barsotti et al., 2015).

61 This study aims at bringing together geological data from different eruptions of different styles at  
62 Somma-Vesuvius to assess and compare the relative magma fragmentation processes, and  
63 characterize their ESPs, which is pivotal for robustly predicting tephra loading and airborne ash  
64 dispersal of future eruptions. Moreover, the quantification of TGSD, including ash, for each  
65 eruption can be used as an indicator for comparing the magma fragmentation efficiency during the  
66 different eruptions, and its effect on the eruptive style at Somma-Vesuvius.

67 Assessing TGSD is also very important for characterizing the eruptive style by associating particle  
68 size distribution to the initial gas content and magma-water interaction processes (e.g. Kaminski  
69 and Jaupart, 1998, Rust and Cashman, 2011, Costa et al., 2016). Commonly, TGSD is required as  
70 key input parameter within tephra dispersal models for reconstructing or predicting the tephra  
71 loading and airborne ash dispersal (e.g. Folch, 2012), and to produce risk mitigation strategies  
72 (Folch et al., 2008; Scollo et al., 2008) for future eruptions (e.g. at Somma-Vesuvius). In this study,  
73 the TGSDs of the Avellino, Pollena, 1906, and 1944 eruptions, from Plinian to sub-Plinian and  
74 Violent Strombolian, are assessed by means of the Voronoi tessellation method (Bonadonna and

119  
120  
121 75 Houghton, 2005), which integrates individual georeferenced grain-size distributions (GSD) for each  
122 76 eruption. We also focussed on estimating the fraction of particle matter finer than 10  $\mu\text{m}$   
123 77 (hereinafter  $\text{PM}_{10}$ ) numerically needed for assessing the content of airborne ash (Poret et al.,  
124 78 2018b), which can potentially affect aviation (e.g., Folch and Sulpizio, 2010; Folch et al., 2012;  
125 79 Sulpizio et al., 2012).

128 80 However, determining TGSD from field samples analysis only can have strong limitations due to  
129 81 the sampling distance from the vent (Costa et al., 2016; Poret et al., 2018b) and the spatial and  
130 82 density distribution of samples along the main axis of the tephra plume (Bonadonna and Houghton,  
131 83 2005; Bonadonna et al., 2015; Spanu et al., 2016). In fact, field-derived TGSD typically tends to  
132 84 underestimate the fraction of either or both the coarse and fine populations (Bonadonna and  
133 85 Houghton, 2005; Rose and Durant, 2009; Scollo et al., 2014; Costa et al., 2016). For encompassing  
134 86 these issues and assessing the related uncertainties we carried out a sensitivity analysis and also  
135 87 described the TGSD as the sum of two lognormal (Gaussian in  $\Phi$ ) and then two Weibull  
136 88 distributions by best fitting the field-based TGSDs (Costa et al., 2016, 2017; Poret et al., 2017;  
137 89 2018b; Mueller et al., 2019; Pedrazzi et al., 2019).

141 90 This paper presents first a brief description of the eruptive history of the Somma-Vesuvius volcano,  
142 91 summarizing the main features of each of the considered eruptions. Then, we report the data and  
143 92 methodology used to estimate the relative TGSDs. Finally, we show the TGSD obtained for each  
144 93 eruption together with the discussion of the main findings.

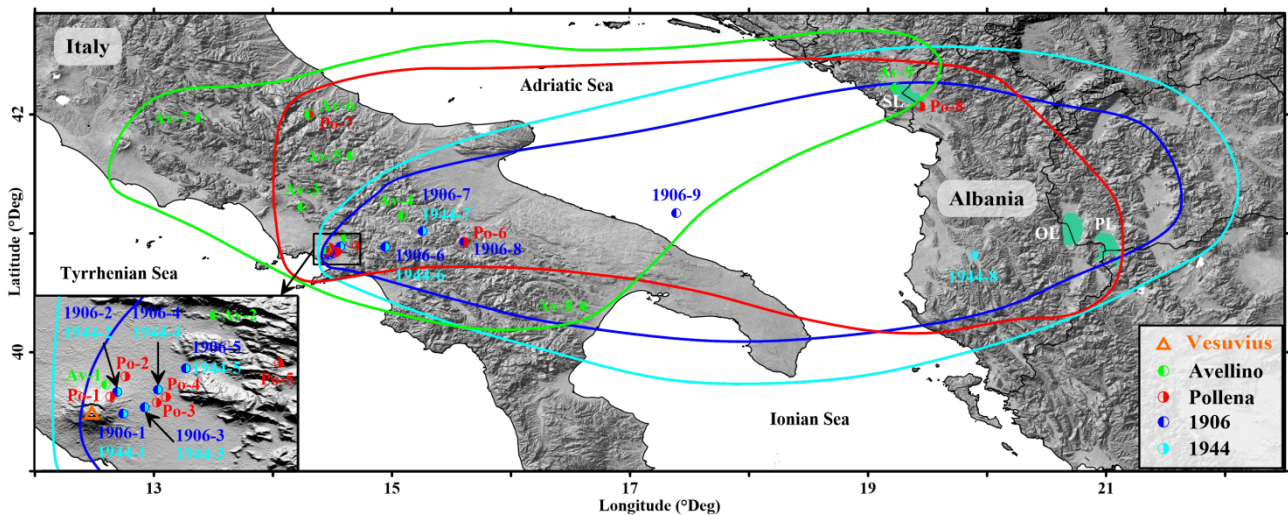
## 147 94 **2 Eruptive history summaries of Somma-Vesuvius and selected eruptions**

149 95 The Somma-Vesuvius eruptive history showed alternating effusive and explosive eruptions,  
150 96 sometimes associated with destructive phases (caldera) of the volcanic edifice. In particular, four  
151 97 Plinian eruptions with caldera collapses truncated the Mt. Somma volcano, forming the present-day  
152 98 summit caldera (Cioni et al., 1999; 2008; Rolandi et al., 2004; Santacroce et al., 2008).  
153 99 Chronologically, these are the Pomici di Base ( $22.03 \pm 0.18$  cal ky BP; Bertagnini et al., 1998;  
154 100 Santacroce et al., 2008), Mercato ( $8.89 \pm 0.09$  cal ky BP; Santacroce et al., 2008; Mele et al., 2011),  
155 101 Avellino ( $3.90 \pm 0.04$  cal ky BP; Sevink et al., 2011; Sulpizio et al., 2010), and Pompeii (A.D. 79;  
156 102 Sigurdsson et al., 1985) eruptions. After the Pompeii eruption, the Vesuvius cone started to grow  
157 103 within the Mt. Somma caldera reaching its present shape (Cioni et al., 2008). Nonetheless, among  
158 104 the recorded post-Pompeii activities, several high-intensity explosive eruptions occurred at Somma-  
159 105 Vesuvius partly modifying the structure of the cone. These are the sub-Plinian Pollena (A.D. 472;  
160 106 Sulpizio et al., 2005) and A.D. 1631 (Poret et al., 2019) eruptions. The most recent period of  
161 107 activity (between A.D. 1631–1944) was characterised by recurrent summit and lateral lava effusions  
162 108 associated with semi-persistent and mild explosive activity, interrupted by pauses lasting from  
163 109 months to a maximum of seven years (Santacroce, 1987; Cioni et al., 2008). During this period,  
164 110 Vesuvius produced a few Violent Strombolian eruptions, such as in 1906 and 1944. In terms of  
165 111 eruption magnitudes (i.e. erupted volume), the literature for the Somma-Vesuvius eruptions reports  
166 112 volumes ranging from 1 to 10  $\text{km}^3$  for Plinian, 0.01 to 1  $\text{km}^3$  for sub-Plinian, and 0.001 to 0.01  $\text{km}^3$   
167 113 for Violent Strombolian eruptions (Cioni et al., 2008).

178  
 179  
 180 114 Hereinafter, we report a synthetic description of the main features of the eruptions considered in the  
 181  
 182 115 present study.

183  
 184 116 **2.1 Avellino and Pompeii Plinian eruptions**

185  
 186 117 The Avellino eruption ( $3.90 \pm 0.04$  cal ky BP; Sevink et al., 2011), was subdivided in three eruptive  
 187 118 phases: opening, magmatic Plinian, and phreatomagmatic (Sulpizio et al., 2010b; 2010c; Massaro et  
 188 119 al., 2018). During the opening phase, a transient short-lived eruptive column reached 12-20 km,  
 190 120 followed by the formation of pyroclastic density currents (PDC) from partial or total collapse of the  
 191 121 eruptive column (Sulpizio et al., 2010c). The magmatic Plinian phase produced a sustained eruptive  
 192 122 column growing with time from 22 to 30 km. This phase ejected the main volume of tephra  
 193 123 estimated at  $1.4 \text{ km}^3$ , which was dispersed mostly north-eastwards (Cioni et al., 2003a; Sulpizio et  
 194 124 al., 2008; 2010c). Finally, the phreatomagmatic phase was dominated by PDC deposits, which  
 195 125 significantly contributed to the total erupted volume with  $\sim 1 \text{ km}^3$  (Sulpizio et al., 2008; 2010a;  
 196 126 2014; Gurioli et al., 2010). It is worth noting that tephra from the Plinian phase was recovered as far  
 197 127 as in Albania (Fig. 1), where they occur within the sedimentary succession of Shkodra lake ( $\sim 430$   
 200 128 km from the source; Sulpizio et al., 2010a).



217 129 **Fig. 1:** Map of the main outcrops of the Avellino, Pollena, 1906, and 1944 Somma-Vesuvius eruptions. The left-bottom inset zooms  
 218 130 onto the proximal area. Coloured lines refer to the dispersal area for each eruption, modified after Sulpizio et al., 2010a, 2010b;  
 219 131 2010c; 2014 for Avellino; Sulpizio et al., 2005; 2010a; 2010c; 2014 for Pollena; Arrighi et al., 2001; Barsotti et al., 2015 for 1906; and  
 220 132 Imbò, 1949; Cole and Scarpati, 2010; Cubellis et al., 2013 for 1944. SL, OL, and PL refer respectively to the Shkodra, Ohrid, and  
 221 133 Prespa lakes (Albania and FYROM). For the interpretation of the references to colour in this figure legend, the reader is referred to  
 222 134 the web version of this article.

222 135 Concerning the Pompeii (A.D. 79) Plinian eruption of Somma-Vesuvius, very famous for the  
 223 136 destruction of the Roman towns of Pompeii and Herculaneum, the volcanological aspects have been  
 224 137 described by numerous authors (e.g. Sigurdsson et al., 1985, Carey and Sigurdsson, 1987,  
 225 138 Macedonio et al., 1988; Pfeiffer et al., 2005). After a short initial phreatomagmatic vent-opening  
 226 139 phase, the eruption was characterized by a purely magmatic phase with a high sustained eruption  
 227 140 column, which was subdivided into a lower layer of white phonolitic pumice (White Pumice) and  
 228 141 an upper tephritic-phonolitic pumice fall (Gray Pumice) deposit. This phase ended column collapse  
 229 142 and the emplacement of pyroclastic flows, which was followed by □phreatomagmatic activity and  
 230 143 the emplacement of lithic-rich breccia and pyroclastic surges, interpreted as the consequence of  
 231 144 decreasing pressure in the vent and magma-water interaction. For the White and the Gray units,  
 232  
 233  
 234  
 235  
 236

237  
238  
239  
240  
241  
242  
243  
244  
245  
246  
247  
248  
249  
250  
251  
252  
253  
254  
255  
256  
257  
258  
259  
260  
261  
262  
263  
264  
265  
266  
267  
268  
269  
270  
271  
272  
273  
274  
275  
276  
277  
278  
279  
280  
281  
282  
283  
284  
285  
286  
287  
288  
289  
290  
291  
292  
293  
294  
295

145 Sigurdsson et al. (1985) estimated, respectively,  $2.5 \times 10^{12}$  and  $6.5 \times 10^{12}$  kg of tephra, or 1 and 2.6  
146 km<sup>3</sup> DRE. Concerning the column height, they estimated that during the White Pumice phase it  
147 increased from about 15 to 26 km, while during the Gray phase, it reached to a maximum of 32 km  
148 and then decreased to about 27 km.

## 149 **2.2 Pollena sub-Plinian eruption**

150 The Pollena eruption (A.D. 472) is the major sub-Plinian event of Somma-Vesuvius, and is  
151 considered by Italian Civil Protection as one of the reference scenarios in case of renewal of  
152 explosive activity. Sulpizio et al. (2005) described the eruption through three phases (i.e. opening,  
153 magmatic and phreatomagmatic), with a similar eruptive evolution to that described for the Plinian  
154 events. In particular, the Pollena eruption was characterized by a highly unstable MER during the  
155 opening phase, resulting in eruptive column pulses with general dispersal of the tephra fallout  
156 deposit towards north-east. Then, during the magmatic phase, at least two dominant pulses of high  
157 eruptive intensity are recorded by the deposition of pyroclastic fall beds and by the signature of  
158 dilute and dense PDCs (Sulpizio et al., 2005). The MER reached a peak intensity of  $\sim 3.4 \times 10^7$  kg/s  
159 during this phase, in particular during the emplacement of the L<sub>8</sub> fallout bed, which is the most  
160 dispersed (Sulpizio et al., 2005). The final phreatomagmatic phase was characterized by a pulsating  
161 column and emplacement of diluted to concentrated PDCs.

162 The tephra fallout deposits dispersed north-eastwards (Fig. 1; see also Sulpizio et al., 2005), while  
163 the PDCs deposited mainly on the northern slopes of the volcano. It is worth noting that fine ash  
164 reached the Balkans, being identified in the sedimentary succession of the Shkodra lake ( $\sim 440$  km  
165 from the source; Sulpizio et al., 2010a), and as crypto-tephra in Ohrid lake (Sulpizio et al., 2010c).  
166 Sulpizio et al. (2005) estimated the volume of the pyroclastic fall deposits around 0.44 km<sup>3</sup> using  
167 the proximal isopachs. Such a volume increases up to  $\sim 1.38$  km<sup>3</sup> and the maximum column height  
168 around 28 km by adding data from distal sites (Sulpizio et al., 2005).

## 169 **2.3 The 1906 and 1944 Violent Strombolian eruptions**

170 The 1906 and 1944 eruptions are examples of Violent Strombolian eruptions at Somma-Vesuvius,  
171 which are typically characterized by emplacement of lava flows in the early phases followed by  
172 explosive activities (Imbò, 1949; Cioni et al., 2008). The latter phases of the eruptions typically  
173 consist of intense lava fountaining episodes associated with eruptive columns rising up to several  
174 kilometre heights. Sometimes, a phreatomagmatic phase closed the activity, accompanied by ash  
175 emissions. The Violent Strombolian eruptive style is considered the most likely scenario in the case  
176 of a possible future reactivation of Somma-Vesuvius (Marzocchi et al., 2004; Neri et al., 2008). In  
177 particular, the eruptions of 1906 and 1944 produced tephra deposits of metric thickness in proximal  
178 areas, with distal ash deposits recognized as far as in Albania (Cubellis et al., 2013).

179 Several overviews and details of the 18-day long 1906 eruption are available in the literature (e.g.  
180 De Lorenzo, 1906; Mercalli, 1906; Sabatini, 1906; Perret, 1924; Bertagnini et al., 1991; Scandone  
181 et al., 1993; Barsotti et al., 2015). The eruption started with a 4-day effusive-explosive phase; then  
182 an intense lava fountaining episode occurred and the Violent Strombolian phase started, lasting 2  
183 days (Mercalli, 1906; Barsotti et al., 2015 – Phase I) and producing a column that reached  $\sim 13$  km

296  
297  
298  
299  
300  
301  
302  
303  
304  
305  
306  
307  
308  
309  
310  
311  
312  
313  
314  
315  
316  
317  
318  
319  
320  
321  
322  
323  
324  
325  
326  
327  
328  
329  
330  
331  
332  
333  
334  
335  
336  
337  
338  
339  
340  
341  
342  
343  
344  
345  
346  
347  
348  
349  
350  
351  
352  
353  
354

184 above the vent (Perret, 1924; Scandone et al., 1993). Ash emissions dispersed towards the Adriatic  
185 Sea (Arrighi et al., 2001) and Montenegro (~400 km from the vent; De Lorenzo, 1906; Barsotti et  
186 al., 2015), as shown by the tephra fallout extent displayed in Fig. 1. Finally, a 12-day long phases of  
187 ash emission (Barsotti et al., 2015 – Phase II) occurred releasing abundant reddish-grey fine ash  
188 together with millimetre-sized accretionary lapilli (De Lorenzo, 1906; Mercalli, 1906). Wind  
189 conditions alternatively dispersed ash over the city of Naples and surroundings (Hobbs 1906).  
190 Sabatini (1906) estimated a minimum tephra fallout volume of ~0.21 km<sup>3</sup> and Barsotti et al. (2015)  
191 reported a TEM of  $1.34 \times 10^{11}$  kg. Furthermore, they mention a MER of  $10^6$  and  $10^5$  kg/s for Phase  
192 I and II respectively, i.e. a bulk MER of  $10^6$  kg/s. Sulpizio et al. (2012) estimated a TEM at  $9.3 \times$   
193  $10^{10}$  kg and a fallout mass of  $3.7 \times 10^{10}$  kg. For a duration of 18 days, the average MER is estimated  
194 at  $6 \times 10^4$  kg/s. In contrast, Cioni et al. (2008; references therein) report a peak MER of  $3.4 \times 10^5$   
195 kg/s for the basal lapilli bed and  $5.4 \times 10^6$  kg/s for the paroxysmal phase.

196 The 17-day long 1944 eruption started with the emplacement of lava flows mainly towards the  
197 north slopes of the actual Vesuvius cone. The subsequent explosive phase comprises a series of 8  
198 lava fountains over a time interval of ~8 h (Arrighi et al., 2001). Scandone et al. (1993) report for  
199 this phase a steady eruptive column that reached ~5 km above the vent and ejected ash into the  
200 atmosphere (Macedonio et al., 2008). In particular, Imbò (1949) provided information relative to  
201 the meteorological conditions. The tephra was transported towards south-east (Fig. 1), reaching  
202 Albania where ash fallout has been observed in Devoli (Cubellis et al., 2013). Cioni et al. (2008)  
203 estimated the erupted volume at ~0.066 km<sup>3</sup> from the isopachs map produced by Pesce and Rolandi  
204 (2000). Based on the TEM estimated at  $2.2 \times 10^{12}$  kg and the eruption duration (17 days), the  
205 average MER is estimated at  $1.5 \times 10^6$  kg/s (Cioni et al., 2008). Differently, Scandone et al. (1986)  
206 report a MER of  $4 \times 10^5$  kg/s, whereas Macedonio et al. (2008) estimated the MER at  $5 \times 10^5$  kg/s  
207 for modelling tephra fallout.

### 208 **3 Data and Methodology**

#### 209 **3.1 Field data**

210 To reconstruct the dispersal of tephra deposits of the studied eruptions (Fig. 1), we used geological  
211 data from literature (e.g. Imbò, 1949; Arrighi et al., 2001; Cioni et al., 2003a; Sulpizio et al., 2005;  
212 2007; 2010a; 2010b; 2010c; 2010d; 2012; 2014; Cole and Scarpati, 2010; Cubellis et al., 2013;  
213 Barsotti et al., 2015). Throughout the manuscript, we will use the terms proximal, medial, and distal  
214 for indicating the areas affected by tephra at different distances. Nonetheless, these zones reflect the  
215 distance from the vent and strongly depend on the eruption intensity (i.e. the column height)  
216 together with the atmospheric conditions (e.g. wind fields). Costa et al. (2016) proposed to consider  
217 distances from 1/10 to 10 times the eruptive column height to define the proximal, medial, and  
218 distal deposits, for adequately sampling the whole tephra fallout up to 125 µm (although such  
219 distances depend on wind conditions as discussed in their work). In this study, for the sake of  
220 simplicity, we use the term proximal to indicate distances from the source up to 30 km, medial for  
221 distances of 30-200 km, and distal for distances > 200 km.

222 Field data comprise tephra samples collected for the Avellino, Pollena, 1906, and 1944 eruptions  
223 (Fig. 1; Table 1). All the details are available as Supplementary Material (Tables S1, S2, S3, and S4

224 respectively for the Avellino, Pollena, 1906, and 1944 eruptions). Regarding the Avellino eruption,  
 225 we used 9 samples distributed from proximal (samples 1-2), to medial areas (samples 3-8) derived  
 226 from Sulpizio et al. (2010b), and a distal one in the Shkodra lake (sample 9; Sulpizio et al., 2010a).  
 227 The Pollena fallout deposits were characterized using 8 samples distributed in proximal (samples 1-  
 228 5), medial (samples 6-7), and distal areas (sample 8 in the Shkodra lake, Albania; Sulpizio et al.,  
 229 2010a). Recently, ash related to the Pollena eruption was also reported as crypto-tephra in the Ohrid  
 230 lake (Albania and FYROM border; Vogel et al., 2009; Sulpizio et al., 2010d), expanding  
 231 significantly the tephra deposit eastwards (Fig. 1). However, the lack of grain-size analysis prevents  
 232 from integrating data for this outcrop.

233 **Table 1:** Field measurements (i.e. location, distance from the vent, main mode, and loading) used for the grain-size analysis and  
 234 TGSD estimations of the Avellino, Pollena, 1906, and 1944 eruptions at Somma-Vesuvius. Sample locations are shown in Fig. 1.  
 235 Details of the field data are available as Supplementary Material (Tables S1, S2, S3, and S4).

Samples		Field observations			
Avellino	Longitude	Latitude	Distance (km from source)	Mode ( $\Phi$ )	Loading (kg/m <sup>2</sup> )
Av-1	14.447	40.867	5	-3	$1.80 \times 10^2$
Av-2	14.611	40.971	23	-2	$1.40 \times 10^2$
Av-3	14.245	41.223	47	3	$3.00 \times 10^1$
Av-4	15.091	41.151	67	1	$1.20 \times 10^2$
Av-5	14.661	41.654	94	2	$4.00 \times 10^1$
Av-6	14.305	42.001	131	5	$3.00 \times 10^1$
Av-7	13.385	41.974	155	4	$3.00 \times 10^1$
Av-8	16.619	40.388	191	5	$3.00 \times 10^1$
Av-9	19.232	42.228	430	5	$1.00 \times 10^1$
<b>Pollena</b>					
Po-1	14.454	40.849	4	-3	$3.84 \times 10^2$
Po-2	14.477	40.879	8	-2	$1.30 \times 10^2$
Po-3	14.524	40.839	9	-3	$1.40 \times 10^2$
Po-4	40.848	14.538	10	-3	$1.30 \times 10^2$
Po-5	14.708	40.899	25	-1	$1.68 \times 10^2$
Po-6	15.605	40.930	100	2	$3.50 \times 10^1$
Po-7	14.305	42.001	130	3	$1.00 \times 10^1$
Po-8	19.440	42.070	440	6	$5.00 \times 10^1$
<b>1906</b>					
1906-1	14.473	40.823	4	-2	$5.50 \times 10^2$
1906-2	14.464	40.856	5	-2	$5.50 \times 10^2$
1906-3	14.506	40.833	7	0	$2.75 \times 10^2$
1906-4	14.526	40.859	10	-2	$1.10 \times 10^2$
1906-5	14.567	40.891	14	-3	$1.10 \times 10^2$
1906-6	14.946	40.887	44	1	$1.10 \times 10^1$
1906-7	15.258	41.019	72	2	$5.50 \times 10^0$
1906-8	15.605	40.931	100	3	$2.20 \times 10^0$
1906-9	17.388	41.173	252	3	$4.40 \times 10^0$
<b>1944</b>					
1944-1	14.473	40.823	4	-2	$6.00 \times 10^2$
1944-2	14.464	40.856	5	-2	$6.00 \times 10^2$
1944-3	14.506	40.833	7	-1	$3.00 \times 10^2$
1944-4	14.526	40.859	10	-1	$1.20 \times 10^2$
1944-5	14.567	40.891	14	-3	$1.00 \times 10^1$
1944-6	14.946	40.887	44	1	$1.20 \times 10^1$
1944-7	15.258	41.019	72	2	$6.00 \times 10^0$
1944-8	19.883	40.814	460	5	$1.20 \times 10^0$

414  
415  
416 237 For the 1906 and 1944 Violent Strombolian eruptions, 7 samples were collected at the same  
417 238 locations (Table 1), representing the proximal (samples 1-5) and medial areas (samples 6-7). Then,  
418 239 the samples 8 and 9 of the 1906 eruption were collected in the Monticchio lake and in a marine core  
420 240 offshore the city of Bari (Fig. 1), located at ~100 and ~252 km from the source respectively. The  
421 241 data related to these samples are reported in Fig. 1 and Table 1. For the 1944 eruption, the farthest  
422 242 sample (sample 8) was collected in Devoli (Albania; Cubellis et al., 2013), which is ~460 km from  
423 243 the vent.  
424 243

### 425 426 244 **3.2 Estimating the TGSDs** 427

428 245 Sampling data include measurements of the tephra loading at several sites (Fig. 1 and Table 1),  
429 246 which were sieved for assessing the GSDs relative to the affected areas. The sieving method gives  
430 247 GSD from -5 to 5  $\Phi$  (Poret et al., 2018a), where  $\Phi = -\log_2 d$  with  $d$  is the particle diameter in  
432 248 millimetre (Krumbein, 1934). Meanwhile, fine ash was analysed through the Beckman Coulter  
433 249 Counter Multisizer<sup>TM</sup> 4 at the University of Bari, Italy. The latter method gives GSD from 3 to 7  $\Phi$ ,  
435 250 extending the grain-size analysis towards the tail of the distribution relative to fine ash. The  
436 251 resulting normalized GSD is obtained by integrating the two partial GSDs taking the sieving  
437 252 method as reference. A similar procedure was successfully used in Poret et al. (2018b) for grain-  
438 253 size purposes integrating complementary methods. Each GSD includes tephra information relative  
440 254 to the bombs (or blocks; diameter  $d \geq 64$  mm), lapilli ( $2 \text{ mm} \leq d < 64$  mm), and ash ( $d < 2$  mm).  
441 255 We further distinguish coarse ash,  $64 \mu\text{m} \leq d < 2$  mm, and fine ash,  $d < 64 \mu\text{m}$  (e.g., Folch, 2012).  
442 255

443 256 Among the several integration methods existing for estimating TGSD (e.g. weighted average,  
444 257 Walker et al., 1981; sectorization of the deposit, Carey and Sigurdsson, 1982; isomass maps,  
445 258 Murrow et al., 1980), in this study we use the Voronoi tessellation method (Bonadonna and  
446 259 Houghton, 2005), considering its advantages and limitations (Bonadonna and Houghton, 2005;  
448 260 Bonadonna et al., 2015; Costa et al., 2016; Spanu et al., 2016; Poret et al., 2018a; 2018b). The  
449 261 method consists in dividing the pyroclastic deposit into Voronoi polygons associated with each  
451 262 georeferenced GSD (i.e. each sample). Then, TGSD is obtained as the weighted average of the mass  
452 263 distribution over the Voronoi cells, which refer to the entire deposit. Prior to apply this method, it is  
453 264 fundamental to define the areal extent of the tephra deposit through assessment of the zero-line  
454 265 contour, which is the line at which the deposit thickness can be assumed negligible (literally equal  
456 266 to zero; Bonadonna and Houghton, 2005). In the studied cases, we used the data from the literature  
457 267 to assess the zero contours (see Fig. 1). Starting from the field-based TGSDs of the different  
458 268 eruptions, we also inferred the TGSDs by means of general analytical distributions (Costa et al.,  
459 269 2016; 2017). First, we considered the sum of two lognormal distributions (hereinafter bi-Gaussian  
461 270 in  $\Phi$ -units):  
462 270

$$463 \quad 464 \quad 271 \quad f_{bi-Gaussian}(\Phi) = p \frac{1}{\sigma_1 \sqrt{2\pi}} e^{-\frac{(\Phi - \mu_1)^2}{2\sigma_1^2}} + (1 - p) \frac{1}{\sigma_2 \sqrt{2\pi}} e^{-\frac{(\Phi - \mu_2)^2}{2\sigma_2^2}}$$

466 272 where  $\Phi$  denotes particle diameter,  $p$  and  $(1-p)$  are, respectively, the coarse and fine sub-population  
468 273 weights, and  $\mu_1$ ,  $\mu_2$  and  $\sigma_1$ ,  $\sigma_2$  denote the mean and standard deviation of the two Gaussian  
469 274 distributions in  $\Phi$ -units. Then, we used two Weibull distributions (Costa et al., 2016; 2017):  
470 274  
471  
472

$$f_{bi-Weibull}(d) = q \frac{1}{n_1 \frac{1}{n_1} \Gamma\left(1 + \frac{1}{n_1}\right)} \frac{1}{\lambda_1} \left[\frac{d}{\lambda_1}\right]^{n_1} e^{-\frac{1}{n_1} \left(\frac{d}{\lambda_1}\right)^{n_1}} + (1-q) \frac{1}{n_2 \frac{1}{n_2} \Gamma\left(1 + \frac{1}{n_2}\right)} \frac{1}{\lambda_2} \left[\frac{d}{\lambda_2}\right]^{n_2} e^{-\frac{1}{n_2} \left(\frac{d}{\lambda_2}\right)^{n_2}}$$

where  $d$  denotes particles diameter,  $q$  and  $(1-q)$  are, respectively, the coarse and fine sub-population weights, and  $\lambda_1, \lambda_2$  and  $n_1, n_2$  are the scale and shape parameters of the two distributions.

## 4 Results and discussions

### 4.1 Individual grain-size distributions

The results for the individual GSDs are displayed in Figs. 2, 3, 4 and 5, respectively for the Avellino, Pollena, 1906, and 1944 eruptions. First of all, it is worth noting that all the TGSD reconstructions (Fig. 6) reflect the limitations associated with the available tephra samples in terms of number and spatial distribution. Moreover, such a reconstruction suffers from the fact that all kinds of tephra particles are considered together, without distinguishing for the different lithologies, which can have different settling behaviours. However, the reconstructed TGSDs represent the best approximations of the initial magma fragmentation for each of the studied eruptions.

Regardless of the eruption, the GSDs at each location show a unimodal distribution with a clear shift of the mode from proximal to distal areas. Such features have been typically observed for several tephra fallout deposits (e.g. Durant et al., 2009; 2010 for the 1980 Mt. St. Helens eruption; Watt et al., 2015 for the Chaiten eruption). Considering the proximal samples (Fig. 1; Table 1), regardless of the eruption, the modes range from -3 to 0  $\Phi$  (Table 1), with similar size and proportions, indicating a dominance of lapilli and coarse ash up to 30 km from the source, typically having relatively high terminal velocities, and thus depositing near the volcano (Bonadonna and Costa, 2013). Regarding the medial areas, the modes range from 1 to 6  $\Phi$  (Table 1), covering a larger grain-size range than in the proximal area due to a larger sampling distance range (i.e. ~44-191 km from the source), different eruptive column heights (3-30 km), and wind intensities (Costa et al., 2016). In particular, for the Pollena, 1906, and 1944 eruptions, the modes vary from 1 to 3  $\Phi$  (see Figs. 3, 4, 5, and Table 1), whereas the Avellino eruption has medial modes up to 6  $\Phi$  (Fig. 2 and Table 1). Indeed, only the Avellino eruption deposits have medial samples up to ~191 km from the vent. Furthermore, samples at similar distances from the source tend to indicate the same modes, being consistent with the main findings of Spanu et al. (2016). Considering the distal samples, modes range between 5 to 6  $\Phi$ , except for the 1906 distal sample (i.e. 3  $\Phi$ ; Fig. 4 and Table 1), which is closer to the vent than for the other eruptions (i.e. ~252 km from the source instead of ~430-460 km). It is worth noting that the relative GSDs indicate a good preservation of the tephra fallout for the studied eruptions, mostly made of fine ash (including PM<sub>10</sub>) collected beyond the Apennines and Adriatic Sea up to Albania and Montenegro (Fig. 1; Sulpizio et al., 2010a; 2010d).

532  
533  
534  
535  
536  
537  
538  
539  
540  
541  
542  
543  
544  
545  
546  
547  
548  
549  
550  
551  
552  
553  
554  
555  
556  
557  
558  
559 308  
560 309  
561  
562  
563  
564  
565  
566  
567  
568  
569  
570  
571  
572  
573  
574  
575  
576  
577  
578  
579  
580  
581  
582  
583  
584  
585  
586 310  
587 311  
588  
589  
590

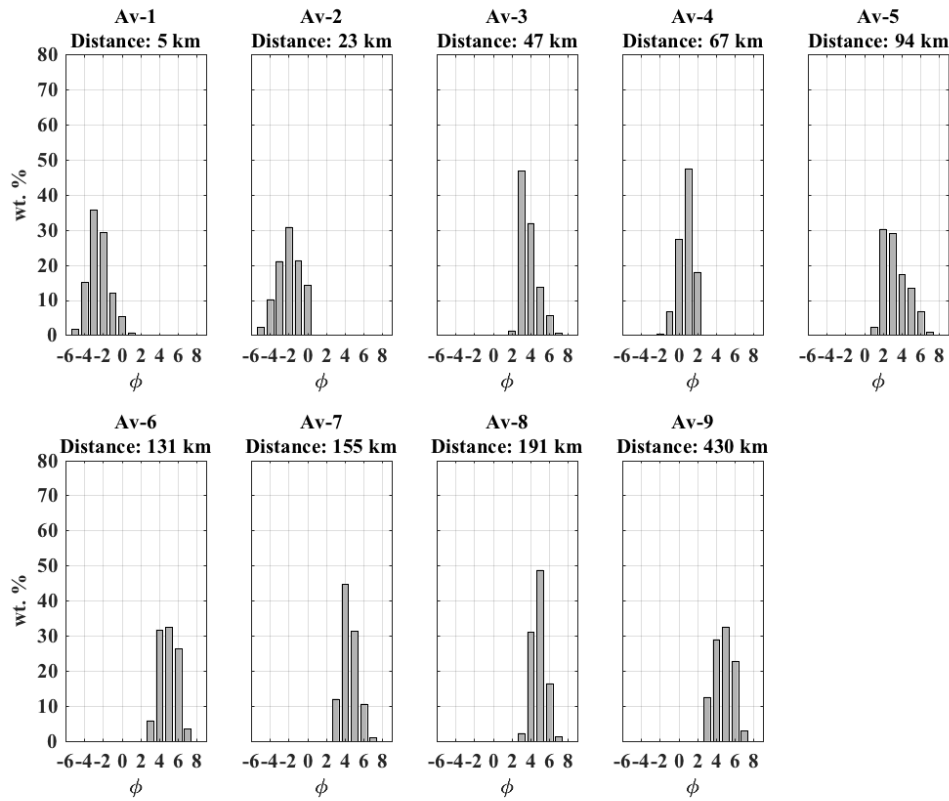


**Fig. 2** Individual field-derived grain-size distributions (samples Av-*x*) for the Avellino Plinian eruption. Sample locations are shown in Fig. 1 and the relative details reported in Table 1. Details of the GSDs are available as Supplementary Material (Table S1).

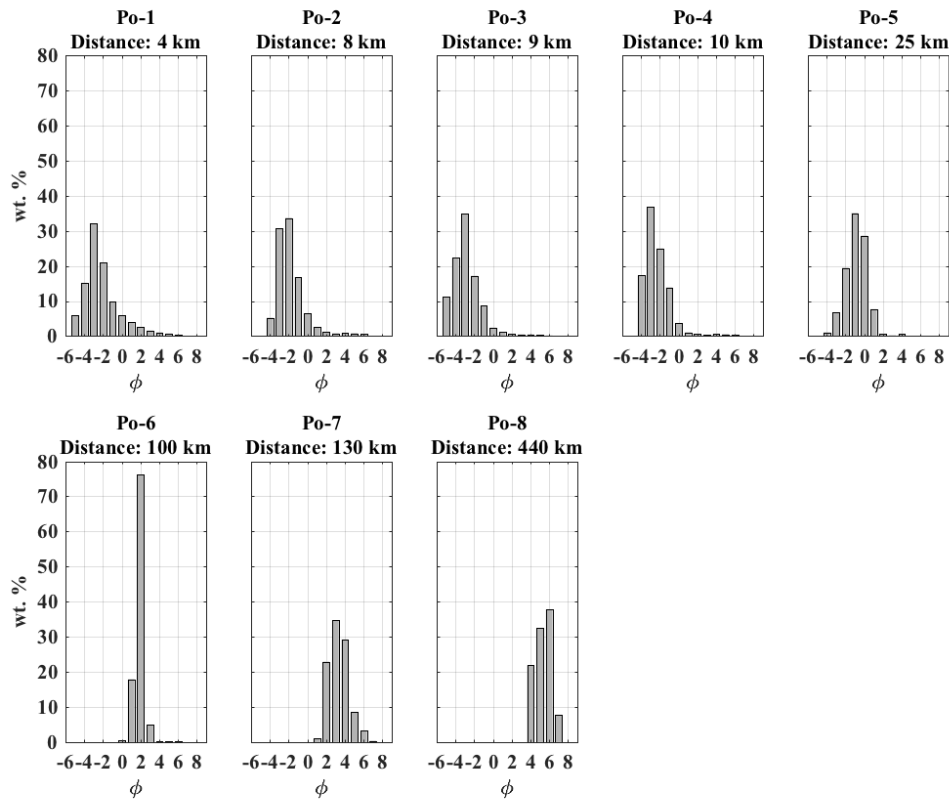


**Fig. 3:** Individual field-derived grain-size distributions (samples Po-*x*) for the Pollena sub-Plinian eruption. Sample locations are shown in Fig. 1 and the relative details reported in Table 1. Details of the GSDs are available as Supplementary Material (Table S2).

591  
592  
593  
594  
595  
596  
597  
598  
599  
600  
601  
602  
603  
604  
605  
606  
607  
608  
609  
610  
611  
612  
613  
614  
615  
616  
617  
618  
619  
620  
621  
622  
623  
624  
625  
626  
627  
628  
629  
630  
631  
632  
633  
634  
635  
636  
637  
638  
639  
640  
641  
642  
643  
644  
645  
646  
647  
648  
649

312 Considering the similarities observed in the evolution of the Plinian and sub-Plinian eruptions (see  
313 Sect. 2), we compare the GSDs of the Avellino (Plinian) and Pollena (sub-Plinian) eruptions (i.e.  
314 Figs. 2 and 3). The proximal areas show similar modes (i.e.  $-3 \Phi$  at  $\sim 5$  km from the source and  
315 between  $-2$  and  $-1 \Phi$  at  $\sim 25$  km), proportions and sizes. Furthermore, we compare the proximal  
316 GSDs of these eruptions with those of the Pompeii Plinian eruption reported in Macedonio et al.  
317 (1988) and collected in Pompeii ( $\sim 11$  km), Castellammare ( $\sim 15$  km), and Maiori ( $\sim 25$  km)  
318 respectively. GSDs have modes at  $-3 \Phi$ , except for Maiori which peaks at  $-2 \Phi$ , being consistent  
319 with the results associated with the Avellino and Pollena eruptions. In the medial zone, samples for  
320 the two eruptions located at  $\sim 100$  km from the source peak at  $2 \Phi$ , and those at  $\sim 130$  km have  
321 modes at  $5$  and  $3 \Phi$  (Table 1), respectively for Avellino and Pollena eruptions. According to  
322 Sulpizio et al. (2008), this feature indicates that a more intense magma fragmentation with high  
323 proportions in fines occurred during the Avellino eruption, especially during the magmatic Plinian  
324 phase. The distal modes for the two eruptions peak between  $5$  and  $6 \Phi$  for samples located in the  
325 Shkodra lake (Albania; Sulpizio et al., 2010a), indicating relatively the same atmospheric  
326 conditions and intensity of magma fragmentation leading to a tephra dispersal towards north-east. It  
327 is worth noting that interpreting grain-size relative to fine ash in terms of intensity of fragmentation  
328 is complex as the energy released at fragmentation depends on the sum of different contributions  
329 and the mechanical strength of the magma (Büttner et al., 2006).

330 Then we compared the GSDs of the 1906 and 1944 Violent Strombolian eruptions (Figs. 4 and 5),  
331 noting that for the proximal and medial areas the tephra fallout appears to be similar in size and  
332 proportion for the same sampling sites (i.e. samples 1-7). Nonetheless, the presence of fine ash at  
333 very proximal distance from the vent (i.e.  $< 4$  km) suggests the likely occurrence of ash aggregation  
334 (Costa et al., 2010; Folch et al., 2010), which appears as disaggregated fine ash at the ground  
335 (Mueller et al., 2017). This observation is supported by Arrighi et al. (2001). The modes change in  
336 distal areas peaking at  $3$  and  $5 \Phi$  respectively for the 1906 and 1944 eruptions (Table 1), due to  
337 different distances from the vent, respectively  $\sim 252$  and  $\sim 460$  km. The literature reports the tephra  
338 fallout of the 1906 eruption in Montenegro (De Lorenzo, 1906; Barsotti et al., 2015; Fig. 1), but  
339 without the possibility of assessing the grain-size distribution due to very thin deposits.

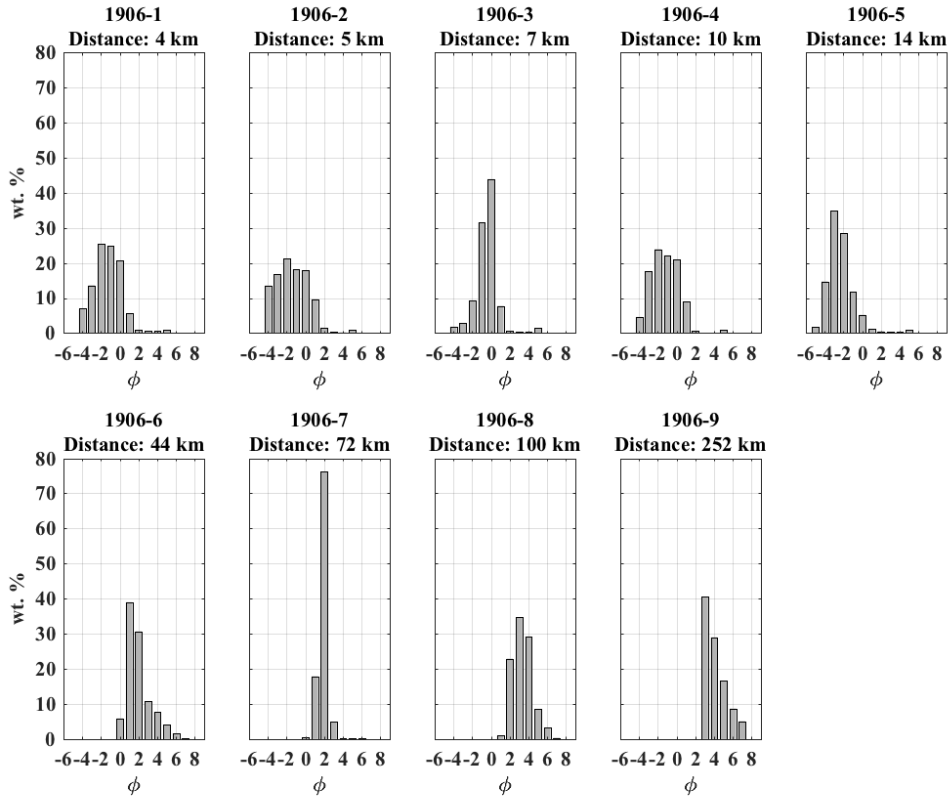


**Fig. 4:** Individual field grain-size distributions (samples 1906-*x*) for the 1906 Violent Strombolian eruption. Sample locations are shown in Fig. 1 and the relative details reported in Table 1. Details of the GSDs are available as Supplementary Material (Table S3).

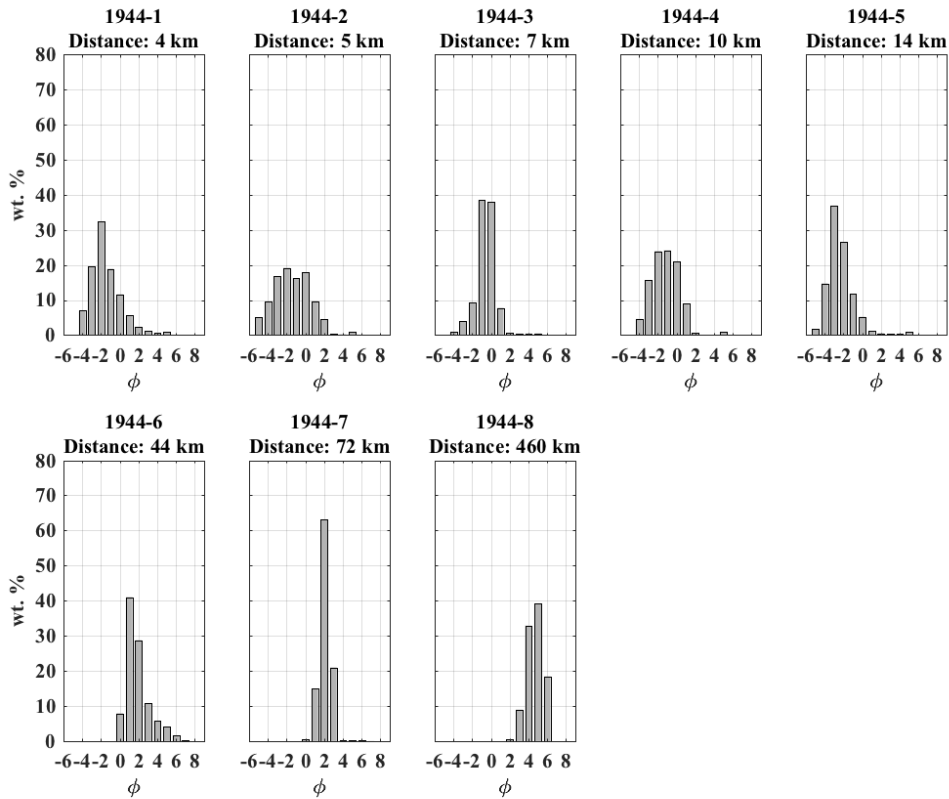


**Fig. 5:** Individual field grain-size distributions (samples 1944-*x*) for the 1944 Violent Strombolian eruption. Sample locations are shown in Fig. 1 and the relative details reported in Table 1. Details of the GSDs are available as Supplementary Material (Table S4).

## 4.2 Total grain-size distributions

In this section, we describe the TGSDs estimated for the studied eruptions by using different methods, such as the Voronoi tessellation method (Bonadonna and Houghton, 2005) or the equivalent bulk grain-size distribution derived from massive PDC deposit (Macedonio et al., 1988; Folch and Sulpizio, 2010), and the analytical parameterizations of the distributions (Costa et al., 2016; 2017). The results give insights into the initial magma fragmentation corresponding to different eruptive styles at Somma-Vesuvius. Although our TGSD estimations are not based on a large number of data in terms of spatial distribution, the dataset covers proximal, medial and distal outcrops for all the studied eruptions. This is quite important as, irrespectively of the eruption style, the lack of distal grain-size data can introduce a significant bias in the TGSD underestimating the fines (e.g.  $PM_{10}$ ) and, hence, preventing the assessment of the airborne ash, which can pose severe hazards to the air traffic (Guffanti et al., 2005; Folch and Sulpizio, 2010; Sulpizio et al., 2014) and public health (Tomašek et al., 2016; 2018).

As already mentioned, TGSDs are first estimated from field data analysis only (Fig. 6). They indicate an overall bimodality pattern, except for the 1944 eruption. In particular, the Avellino field-derived TGSD peaks at 1 and 4  $\Phi$ , respectively for the coarse and fine sub-populations, the Pollena TGSD shows modes at -1 and 6  $\Phi$ , and the 1906 TGSD has modes at 0 and 3  $\Phi$ . For comparison, the TGSD of the Pompeii Plinian eruption (from Macedonio et al., 2008) peaks at 1 and 5  $\Phi$ , in agreement with the TGSDs derived for the Avellino Plinian and Pollena sub-Plinian eruptions. For comparison, the Pollena TGSD estimated assuming an equivalent bulk grain-size distribution derived from massive PDC deposits by Folch and Sulpizio (2010) peaks at 1 and 4-5  $\Phi$ , consistently with the estimations made for the Avellino and Pompeii TGSDs. Differently from the other eruptions, the 1944 TGSD yields a unique mode at -2  $\Phi$ , more similar to the lower intensity and lower magma viscosity eruptions (Costa et al., 2016). Considering the different eruptive styles of the studied cases, the resulting field-based TGSDs indicate modes shifting towards the fines when the eruption intensity increases, in agreement with the analysis performed in Costa et al. (2016).

The TGSDs estimated through the Voronoi tessellation method were obtained after a careful investigation of the effects of the zero-line contour. In fact, TGSD assessment depends on several factors, such as a suitable number of samples well dispersed along the main tephra dispersal (i.e. proximal, medial, and distal areas), but also on the tephra edge defined as the zero-line (Bonadonna and Houghton, 2005; Bonadonna et al., 2015). For optimizing the TGSD estimate, we used the dispersals of the eruptions available in the literature (see Sect. 2) for constraining the tephra extents for each studied eruption. Volentik et al. (2010) studied the uncertainty related to the position of the zero-line, yielding uncertainties on the standard deviation of the modes and the fine ash contained within the TGSD. Nonetheless, Bonadonna et al. (2015) highlighted that these uncertainties are much higher when tephra deposits are not sampled correctly, i.e. including sites up to distal area.

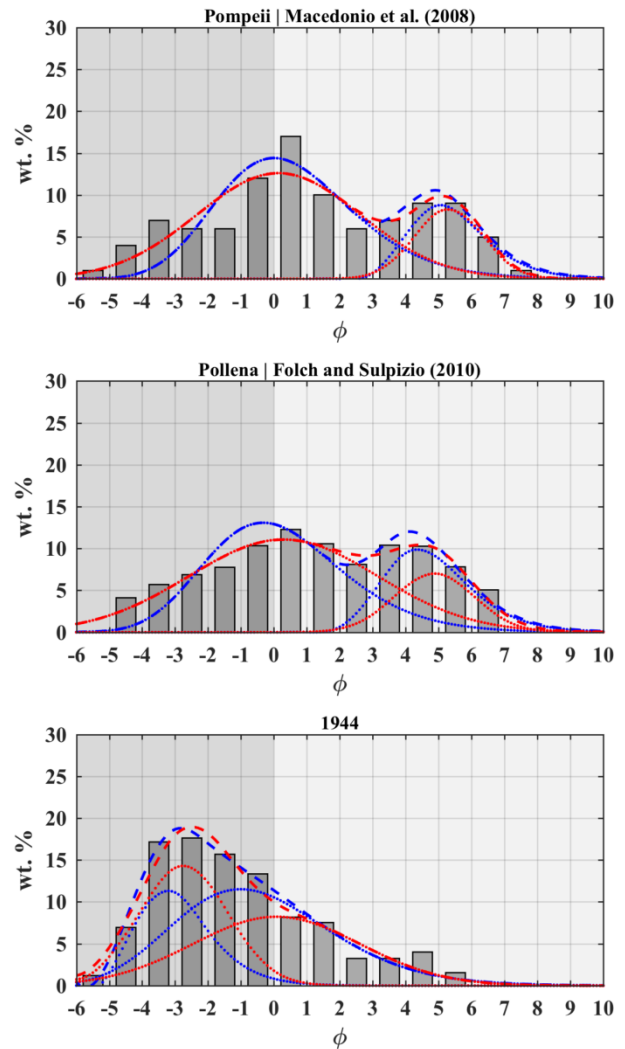
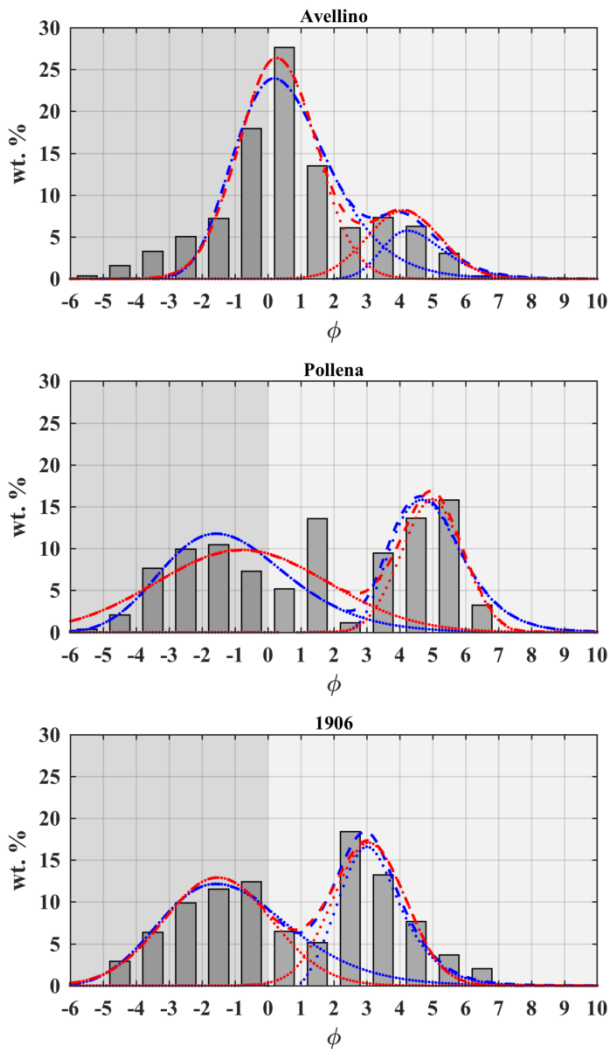


**Fig. 6:** Field-based TGSDs (bars) for the Avellino, Pollena, 1906, and 1944 eruptions. Red lines show the bi-Gaussian distributions best fitting the field TGSDs, and the blue lines the bi-Weibull distributions. The dotted lines refer to the corresponding sub-populations of the relative distributions. Further details on the distributions in Sect. 3.2, and Tables 2, 3 and 4. The field-based TGSD for the Pompeii eruption is from Macedonio et al. (2008) and is used for comparison with the TGSD of the Avellino eruption. The second field-based TGSD for the Pollena eruption is derived from massive PDC deposits by Folch and Sulpizio (2010) and is used for comparison purpose with the Avellino and Pollena eruptions. Grey colours are consistent with Tables 3 and A (see Appendix).

Among tephra, very fine ash (e.g.  $PM_{10}$ ) is released into the atmosphere where it can remain for days to weeks dispersing towards distal areas (Rose and Durant, 2009). Such fine material, which escapes to aggregation processes, is very difficult to sample due to the very long residence time in the atmosphere. It follows that  $PM_{10}$  are typically under-sampled, biasing the field-derived TGSDs towards the fines and preventing the correct assessment of the airborne ash mass and the relative concentration (Poret et al., 2018a, 2018b), with implications for the assessment of hazards to the air traffic (e.g., Guffanti et al., 2005). In particular, the present study shows that Plinian eruptions (e.g. Avellino and Pompeii) may produce around 80 wt. % of ash with a  $PM_{10}$  content of few percent (Table 3), which can have a strong impact on the air traffic safety producing extended areas with ash concentration above the threshold of  $4 \text{ mg/m}^3$  (Gouhier et al., 2019 and references therein) delimiting the no-fly zones. It is worth noting that Gouhier et al. (2019) recently demonstrated that the more intense eruptions (i.e. Plinian) are the least efficient in transporting the airborne  $PM_{10}$ , due to early en masse fallout. This explains why we regularly observe ash in proximal and medial areas but also suggests that measured  $PM_{10}$  fractions are the minimum amount to consider. A few studies have attempted to assess such fraction at Etna (Sicily, Italy) integrating field and remote sensing

827  
828  
829  
830  
831  
832  
833  
834  
835  
836  
837  
838  
839  
840  
841  
842  
843  
844  
845  
846  
847  
848  
849  
850  
851  
852  
853  
854  
855  
856  
857  
858  
859  
860  
861  
862  
863  
864  
865  
866  
867  
868  
869  
870  
871  
872  
873  
874  
875  
876  
877  
878  
879  
880  
881  
882  
883  
884  
885

data (i.e. satellite and/or X-band radar retrievals; Poret et al., 2018a, 2018b). Although PM<sub>10</sub> fraction is negligible compared to the bulk tephra, it is critical for operational models (e.g. those used by the Volcanic Ash Advisory Centers) when using the tephra dispersal models.

Considering the time occurrence of the studied eruptions, and the consequent absence of remote sensing data, for trying to better capture the tails of the field-based TGSDs, i.e. fine and coarse, we described the TGSDs by means of bi-Gaussian and bi-Weibull distributions, which allow extrapolations. Overall, all the distributions best fitting the field TGSDs are estimated by assuming two main tephra populations (i.e. a coarse and a fine) as described in Costa et al. (2016; 2017). Indeed, Costa et al. (2016) show that bimodality of TGSDs is a common feature for several tephra fallout deposits. This is also the case of this study, showing asymmetric and clear bimodal signature for all the TGSDs (Fig. 6), except for the 1944 eruption that, although asymmetric, has a more unimodal pattern. However, the obtained TGSDs suggest that bimodality can be due to magma heterogeneity, secondary fragmentation or phreatomagmatism (Jones and Russell, 2017). For better classifying whether TGSDs are bimodal or unimodal, Costa et al. (2016) used a bimodality index (*BI*) for bi-Gaussian distributions as following:

$$BI = \sqrt{2} \frac{|\mu_1 - \mu_2|}{\sqrt{\sigma_1^2 + \sigma_2^2}} \sqrt{p(1-p)}$$

where the parameters  $\mu_i$  and  $\sigma_i$  refer to modes and standard deviations of the Gaussian distributions (Sect. 3.2). The best fitting parameters are reported in Table 2 together with the associated *BI* values.

**Table 2:** Parameterization of the distributions in best fit of the field-based TGSDs for the Avellino, Pompeii, Pollena, 1906, and 1944 eruptions. *p* and (1-*p*) are, respectively, the coarse and fine sub-population weights, and  $\mu_1$ ,  $\mu_2$  and  $\sigma_1$ ,  $\sigma_2$  are the mean and standard deviation of the two Gaussian distributions in  $\Phi$ -units. *q* and (1-*q*) are, respectively, the coarse and fine sub-population weights, and  $\lambda_1$ ,  $\lambda_2$  and  $n_1$ ,  $n_2$  are the scale and shape parameters of the two distributions, respectively. The bimodality is investigated for the Gaussian distributions only through the *BI* (Costa et al., 2016), which is assumed bimodal for *BI* > 1.1. \* TGSD is that used from Macedonio et al. (2008) for comparing with the Avellino eruption. \*\* TGSD is that used by Folch and Sulpizio (2010).

bi-Gaussian						
	Avellino	Pompeii *	Pollena	Pollena **	1906	1944
$\mu_1$ ( $\Phi$ )	0.29 ± 0.07	0.14 ± 0.26	-0.78 ± 0.46	0.28 ± 0.16	-1.52 ± 0.17	-2.74 ± 0.10
$\sigma_1$ ( $\Phi$ )	1.16 ± 0.06	2.48 ± 0.21	2.60 ± 0.38	2.86 ± 0.13	1.64 ± 0.14	1.34 ± 0.08
$\mu_2$ ( $\Phi$ )	4.12 ± 0.23	5.32 ± 0.25	4.99 ± 0.17	4.87 ± 0.16	3.08 ± 0.11	0.08 ± 0.24
$\sigma_2$ ( $\Phi$ )	1.10 ± 0.19	1.04 ± 0.20	0.92 ± 0.14	1.22 ± 0.13	1.10 ± 0.09	2.53 ± 0.20
<i>p</i>	0.77 ± 0.02	0.78 ± 0.03	0.63 ± 0.04	0.79 ± 0.02	0.53 ± 0.03	0.48 ± 0.03
<i>BI</i>	1.41	1.13	1.43	0.85	1.65	0.70
bi-Weibull						
$\lambda_1$ (in mm)	0.41 ± 0.04	0.43 ± 0.07	1.28 ± 0.31	0.54 ± 0.08	1.27 ± 0.12	4.82 ± 0.28
$n_1$	0.65 ± 0.03	0.38 ± 0.01	0.42 ± 0.03	0.37 ± 0.01	0.40 ± 0.01	0.95 ± 0.05
$\lambda_2$ (in mm)	0.03 ± 0.01	0.02 ± 0.01	0.02 ± 0.01	0.02 ± 0.01	0.07 ± 0.01	0.84 ± 0.07
$n_2$	1.16 ± 0.40	0.88 ± 0.15	0.98 ± 0.12	0.75 ± 0.07	1.16 ± 0.06	0.30 ± 0.01
<i>q</i>	0.86 ± 0.04	0.74 ± 0.04	0.56 ± 0.05	0.68 ± 0.04	0.60 ± 0.02	0.32 ± 0.02

First of all, the results associated with the bimodal index (*BI*) reported in Table 2 tends to indicate bimodal distributions for all the TGSDs, except for that of the Pollena eruption estimated from Folch and Sulpizio (2010) and the 1944 distribution. Indeed, their values are below 1.1, suggesting a more unimodal distribution, although these distributions are made by coarse and fine populations, which are close enough for showing a unimodal-like shape of the distributions (Fig. 6).

886  
887  
888  
889  
890  
891  
892  
893  
894  
895  
896  
897  
898  
899  
900  
901  
902  
903  
904  
905  
906  
907  
908  
909  
910  
911  
912  
913  
914  
915  
916  
917  
918  
919  
920  
921  
922  
923  
924  
925  
926  
927  
928  
929  
930  
931  
932  
933  
934  
935  
936  
937  
938  
939  
940  
941  
942  
943  
944

432 Considering that TGSD is needed as input parameter for tephra dispersal models, typically in the  
433 form of discrete size bins, we report the TGSD bins obtained from the field measurements analysis  
434 (i.e. Field TGSD) and the corresponding bi-Gaussian and bi-Weibull distributions for the studied  
435 eruptions in the Appendix (Tables A1-6). Moreover, we discuss below the magma fragmentation  
436 features inferred for each eruption. For the sake of simplicity, Table 3 reports the mass fractions  
437 associated with each grain-size class (i.e. bomb, lapilli, coarse, and fine ash).

438 Putting together the field-based TGSDs and the relative analytical distributions (i.e. bi-Gaussian  
439 and bi-Weibull), results for the Avellino eruption suggest a first mode between 0 and 1  $\Phi$  and a  
440 second mode at 4  $\Phi$ , respectively for the coarse and fine sub-populations (Fig. 6; Table A1). The  
441 Pollena TGSD shows a first mode from -2 to -1  $\Phi$  and a second mode at 5-6  $\Phi$ . As described in  
442 Sect. 2, the Avellino and Pollena eruptions have similar eruptive trends, even if they are classified  
443 as Plinian and sub-Plinian eruptions, respectively. Comparing the relative sub-populations  
444 displayed in Fig. 6, the Pollena TGSD indicates a tephra deposit relatively coarser than for  
445 Avellino, with a greater production of lapilli (~30 and ~18 wt. % respectively; Tables A1 and A2).  
446 In contrast, the Avellino eruption produced substantially more ash than the Pollena one (~80 against  
447 ~60 wt. % of ash respectively; Tables A1 and A3), being an indicator of the efficiency of the  
448 magma fragmentation. Going further in detail, the Avellino eruption produced more coarse ash with  
449 respect to Pollena (~70 vs. ~35 wt. % respectively), whereas the Pollena eruption has more fine ash  
450 (~8 vs. ~30 wt. %). Furthermore, the PM<sub>10</sub> content is greater for the Pollena eruption compared to  
451 Avellino (~4 and ~1 wt. % respectively; Tables A1 and A3), indicating either a more efficient  
452 magma fragmentation for Pollena, although the eruption showed very unstable eruptive conditions,  
453 or a more efficient transport towards distal region, as suggested by Gouhier et al. (2019). It is worth  
454 noting that the magmatic phase of the Avellino eruption was accompanied by an energy drop  
455 affecting magma fragmentation, representing the phreatomagmatic phase (Sulpizio et al., 2008;  
456 2010b) with a lower fraction of fine ash compare to the Pollena eruption. Sulpizio et al. (2005)  
457 explained this as due to magma fragmentation efficiency but also mentioned the occurrence of an  
458 extensive magma-water interaction, which occurred during the final phase, carrying out a strong  
459 control on the eruption dynamics and increasing the fragmentation of magma during the Pollena  
460 eruption.

461 Going further in the comparative analysis, we compared the Avellino field-derived TGSD with the  
462 one of the Pompeii eruption, being both Plinian events. For these purposes, we used the TGSD  
463 estimations reported by Macedonio et al. (1988; 2008) for the Pompeii eruption. Macedonio et al.  
464 (1988; see Fig. 2b therein) estimated the TGSD from an individual GSD obtained from an outcrop  
465 of PDC deposits representative of the collapse of the eruptive column. Concerning the fine ash  
466 content, they considered all the bin fractions corresponding to  $\Phi \geq 5$  all together as fine residual at  
467  $\Phi = 5$ . It follows that we consider only the coarse mode that peaks at 1  $\Phi$ , being consistent with the  
468 Avellino results. Regarding the class fractions, we can see that this TGSD shows a substantial  
469 enrichment in lapilli (~37 wt. % against ~18 wt. % respectively; Table 3), and thus, a depletion in  
470 ash compared to the Avellino eruption (~63 wt. % against ~82 wt. % respectively). Moreover, it  
471 also shows a slight enrichment in fine ash (~14 wt. % against ~10 wt. % respectively). Then,  
472 Macedonio et al. (2008) reported the bulk Pompeii TGSD that they assumed representative of the  
473 Plinian/Sub-Plinian granulometry at Somma-Vesuvius. We also reconstructed such field-based

945  
946  
947  
948  
949  
950  
951  
952  
953  
954  
955  
956  
957  
958  
959  
960  
961  
962  
963  
964  
965  
966  
967  
968  
969  
970  
971  
972  
973  
974  
975  
976  
977  
978  
979  
980  
981  
982  
983  
984  
985  
986  
987  
988  
989  
990  
991  
992  
993  
994  
995  
996  
997  
998  
999  
1000  
1001  
1002  
1003

474 TGSD through a bi-Gaussian and bi-Weibull distribution and they are displayed in Fig. 6 for  
475 comparing them with the Avellino TGSD. It shows a mode at 0-1  $\Phi$  for the coarse population, and  
476 at 5  $\Phi$  for the fine population (Tables A1-2). Although the paucity of field data implies large  
477 uncertainties on the TGSD assessment, the relative TGSDs indicate comparable values for lapilli  
478 and ash (Table 3), suggesting acceptable results. Looking at the class fractions, the Pompeii TGSD  
479 from Macedonio et al. (2008) shows comparable values with respect to the other TGSDs, with ~24  
480 and ~76 wt. % of lapilli and ash, respectively. Among ash, the TGSD indicates ~52 wt. %, 24 wt.  
481 %, and ~6 wt. % of coarse and fine ash, and PM<sub>10</sub>. It follows that all the three estimates for the  
482 Plinian events (i.e. Avellino and Pompeii) are in agreement with a dominance of ash between 60  
483 and 80 wt. % of the magma fragmentation, being consistent with Rose and Durant (2009) who  
484 discussed how silicic eruptions can contain substantial fractions of ash.

485 Similarly to the previous paragraph, we used the TGSD of the Pollena eruption used by Folch and  
486 Sulpizio (2010) for a comparison with our TGSD estimates (see Fig. 6). They obtained the TGSD  
487 on the basis of an individual GSD obtained from an outcrop of PDC deposits representative of the  
488 collapse of the eruptive column. We also best-fitted their field-based TGSD through the bi-  
489 Gaussian and bi-Weibull distributions. The TGSD peaks at 0-1  $\Phi$  and 4  $\Phi$  for the coarse and fine  
490 populations respectively. This is slightly different from our estimate for the Pollena eruption (see  
491 Tables A3-4), which can be attributed to a different method for assessing the TGSD. In fact, based  
492 on our analysis of the field samples, we obtained a TGSD composed of two more marked grain size  
493 populations than for the TGSD of Folch and Sulpizio (2010). In particular, our TGSD suggest a  
494 coarser proximal deposit with ~31 wt. % of lapilli instead of ~25 wt. % by Folch and Sulpizio  
495 (2010). Regarding the class fractions (Table 3), we can see that Folch and Sulpizio (2010) obtained  
496 ~75 wt. % of ash, whereas our TGSD indicates ~69 wt. %. Furthermore, they suggest ~52 wt. %, 23  
497 wt. %, and ~5 wt. % of coarse and fine ash, and PM<sub>10</sub>, while we have ~37 wt. %, 33 wt. %, and ~3  
498 wt. %, respectively. These results are comparable showing an agreement in favour of saying that  
499 during the Pollena eruption magma fragmentation produced around 30 wt. % of lapilli and 70 wt. %  
500 of ash, with ~45 wt. % of coarse ash, ~30 wt. % of fine ash, and ~4 wt. % of PM<sub>10</sub>. In addition,  
501 these results are very similar to those of the Plinian eruptions and reinforce the similarity between  
502 the Plinian and sub-Plinian eruptive styles.

**Table 3:** Fractions of the different classes used in this study: bombs ( $\Phi \leq -6$ ), lapilli ( $-5 \leq \Phi \leq -1$ ), and ash ( $0 \leq \Phi$ ). We further distinguish between coarse ( $4 \leq \Phi \leq 0$ ) and fine ash ( $\Phi \leq 5$ ) as described in Folch (2012). We also reported the  $PM_{10}$  fraction (diameter below  $10 \mu m$ ) as in Poret et al. (2018b). The fractions are expressed in weight percentage (wt. %) and refer to the field-TGSDs, bi-Gaussian, and bi-Weibull distributions for the Avellino, Pollena, 1906, and 1944 Somma-Vesuvius eruptions. Colours are consistent with Tables A (see Appendix) and Fig. 6. \* Pompeii data are extracted from Macedonio et al. (2008) for comparing with the Avellino eruption. \*\* Pollena data are extracted from Folch and Sulpizio (2010) for comparing with Plinian and sub-Plinian eruptions.

	Class	Field-TGSD	bi-Gaussian	bi-Weibull
Avellino	Bombs	0.00	0.00	0.00
	Lapilli	17.62	18.70	19.71
	Ash	82.38	81.29	80.28
	Coarse ash	72.65	73.14	72.15
	Fine ash	9.73	8.15	8.13
	$PM_{10}$	0.35	0.29	0.81
	Total	100	100	100
Pompeii *	Bombs	0.00	0.59	0.00
	Lapilli	23.98	30.29	24.80
	Ash	78.28	69.12	75.20
	Coarse ash	52.11	48.77	52.17
	Fine ash	24.17	20.35	23.03
	$PM_{10}$	6.05	2.95	5.21
	Total	100	100	100
Pollena	Bombs	0.00	1.31	0.12
	Lapilli	30.58	32.53	36.10
	Ash	69.44	66.17	63.79
	Coarse ash	36.71	38.48	35.12
	Fine ash	32.73	27.69	28.67
	$PM_{10}$	3.26	1.71	4.58
	Total	100	100	100
Pollena **	Bombs	0.00	0.99	0.01
	Lapilli	24.53	29.34	26.89
	Ash	75.12	69.67	73.09
	Coarse ash	51.84	50.80	53.12
	Fine ash	23.28	18.87	19.97
	$PM_{10}$	5.10	2.93	4.08
	Total	100	100	100
1906	Bombs	0.00	0.31	0.19
	Lapilli	30.78	38.73	38.10
	Ash	69.22	60.95	61.70
	Coarse ash	55.78	56.72	56.48
	Fine ash	13.44	4.23	5.22
	$PM_{10}$	2.07	0.03	0.40
	Total	100	100	100
1944	Bombs	0.00	1.21	0.42
	Lapilli	58.73	65.92	65.77
	Ash	41.28	32.86	33.80
	Coarse ash	35.66	30.83	31.54
	Fine ash	5.62	2.03	2.26
	$PM_{10}$	0.02	0.27	0.52
	Total	100	100	100

1063  
1064  
1065 511 Regarding the Violent Strombolian eruptions at Somma-Vesuvius, the TGSD reconstructed for the  
1066 512 1906 eruption has a first mode from -2 to 0  $\Phi$  for the coarse sub-population, and a second mode at 3  
1068 513  $\Phi$  for the fine sub-population (Table 3; Fig. 6). The 1944 TGSD presents significant differences  
1069 514 with respect to the 1906 one, showing a unimodal pattern with a main mode between -3 and -2  $\Phi$ .  
1070 515 Indeed, the second mode is not clearly visible from the Field TGSD, characterizing the fine sub-  
1072 516 population and peaking between -1 and 0  $\Phi$  (respectively for the bi-Weibull and bi-Gaussian  
1073 517 distributions), partially overlapping the coarse sub-population (see Fig. 6). Such discrepancy  
1074 518 between the 1906 and 1944 TGSDs can be interpreted as due to the different processes controlling  
1075 519 magma fragmentation, such as the higher intensity and the major phreatomagmatic phase of the  
1077 520 1906 eruption (Costa et al., 2016). In fact, these results, together with the features of the Pollena  
1078 521 TGSD, support the importance of the phreatomagmatic phase in controlling magma fragmentation  
1079 522 (Sulpizio et al., 2010b). As described in Sect. 2.3, the 1906 and 1944 eruptions are similar in terms  
1081 523 of eruptive style. Comparing the class fractions, the 1906 TGSD is substantially depleted in lapilli  
1082 524 than the 1944 one (~31 and ~59 wt. % respectively; Table 3), but enriched in ash (respectively ~69  
1083 525 and ~41 wt. %; Table 3). Accordingly, the literature (Arrighi et al., 2001) reports that the 1944  
1084 526 event produced a large quantity of lapilli. Another feature reported for the 1944 eruption concerns  
1086 527 the production of ash aggregates up to centimetric size (Arrighi et al., 2001). Although aggregation  
1087 528 implies a premature tephra fallout (Durant et al., 2009; Mastin et al., 2016; Poret et al., 2018c), it  
1088 529 also depletes the TGSD in fines (Poret et al., 2017), affecting the grain-size distribution towards the  
1090 530 fine ash. This also depends on the sampling distance from the source as highlighted by Spanu et al.  
1091 531 (2016). Comparing coarse and fine ash, the results indicate a greater production for the 1906  
1092 532 compared to the 1944 eruption (respectively ~56 against ~36 wt. % for the coarse ash, and ~13  
1093 533 against ~6 wt. % for the fine ash; Table 3). Furthermore, the  $PM_{10}$  fractions yield ~2 wt. % and <1  
1095 534 wt. % for the 1906 and 1944 eruptions, respectively.

1096 535 Summarizing the TGSD analyses, the results allow identifying distinctive grain-size features for the  
1098 536 different eruptive styles at Somma-Vesuvius, although the paucity of field data prevents assuming  
1099 537 the reconstructed TGSDs as fully representative of the initial magma fragmentation conditions.  
1100 538 Indeed, results generally indicate that increasing in intensity (i.e. from Violent Strombolian to  
1101 539 Plinian eruptions) tends to move the main modes of the TGSDs towards the fines (Fig. 6 and Tables  
1103 540 A). Such feature was also reported by Costa et al. (2016), who proposed a model for estimating the  
1104 541 TGSD through the bulk magma viscosity and column height. They observed the mode shifting  
1105 542 towards the fines when increasing the magma viscosity and intensity values. In particular, the  
1107 543 Plinian eruptions (e.g. Avellino and Pompeii at Somma-Vesuvius) appear to be the richest in ash  
1108 544 with up to ~82 wt. % (Table 3). In addition, the Pollena sub-Plinian eruption with ~70 wt. % of ash  
1109 545 ( $PM_{10}$  of ~4 wt. %) and the 1906 Violent Strombolian eruption with ~69 wt. % of ash ( $PM_{10}$  of ~2  
1110 546 wt. %) show exceptional magma fragmentation efficiency in contrast with the Avellino, Pompeii,  
1112 547 and 1944 eruptions.

## 1113 1114 548 **5 Conclusions** 1115

1116 549 This study presents grain-size analyses obtained from several tephra samples associated with four  
1117 550 reference eruptions of Somma-Vesuvius, covering different eruptive styles (from Violent  
1118 551 Strombolian to Plinian), aimed to assess the relative TGSD and the impact of magma fragmentation  
1120  
1121

1122  
1123  
1124  
1125  
1126  
1127  
1128  
1129  
1130  
1131  
1132  
1133  
1134  
1135  
1136  
1137  
1138  
1139  
1140  
1141  
1142  
1143  
1144  
1145  
1146  
1147  
1148  
1149  
1150  
1151  
1152  
1153  
1154  
1155  
1156  
1157  
1158  
1159  
1160  
1161  
1162  
1163  
1164  
1165  
1166  
1167  
1168  
1169  
1170  
1171  
1172  
1173  
1174  
1175  
1176  
1177  
1178  
1179  
1180

552 on the eruptive styles. Chronologically, we focus on the Avellino (3900 yr BP) and the Pompeii  
553 (A.D. 79) Plinian eruptions, the Pollena sub-Plinian eruption (A.D. 472), and the 1906 and 1944  
554 Violent Strombolian eruptions. Previous estimations of the Pompeii and Pollena eruptions were  
555 used for comparison purposes in terms of magma fragmentation for a given eruptive style.  
556 Individual field-based grain-size analyses were integrated using the Voronoi tessellation method for  
557 assessing the TGSD relative to each eruption. Besides the estimation of the field-derived TGSDs,  
558 we parameterized the TGSDs using the analytical bi-Gaussian and bi-Weibull distributions. By  
559 comparing the TGSDs associated with the different eruptive styles, our results indicate that  
560 increasing the eruption intensity, i.e. going from Violent Strombolian to Plinian eruptive style, and  
561 the efficiency of magma-water interaction, i.e. from magmatic to phreatomagmatic eruptions,  
562 TGSD modes move towards the fines, enhancing magma fragmentation. This study brings together  
563 similar conclusions in terms of magma fragmentation stated in the literature, reinforcing their  
564 findings and reopening the interest of studying the fragmentation from field data but not limited to.  
565 We believe this study will serve further works focussing on characterizing the tephra distribution  
566 produced by volcanic eruptions worldwide from Violent Strombolian to Sub-Plinian and Plinian  
567 styles. In particular, the main findings of this study can be used for numerically reconstructing past  
568 eruptions or forecasting similar eruptive scenarios at Somma-Vesuvius, and assessing tephra  
569 loading and/or airborne ash mass from the source towards distal regions.

## 1148-570 **Acknowledgements**

1150  
1151  
1152  
1153  
1154  
1155  
1156  
1157  
1158  
1159  
1160  
1161  
1162  
1163  
1164  
1165  
1166  
1167  
1168  
1169  
1170  
1171  
1172  
1173  
1174  
1175  
1176  
1177  
1178  
1179  
1180

571 This work has been partially supported by the FP 7 Marie Curie Actions Framework (FP7-  
572 PEOPLE-2013- ITN), volcanic ash: field, experimental, and numerical investigations of processes  
573 during its lifecycles (VERTIGO project; grant agreement number 607905). A.C. acknowledges the  
574 European project EUROVOLC (grant agreement number 731070) and the Ministero dell'Istruzione,  
575 dell'Università e della ricerca (MIUR, Roma, Italy) Ash-RESILIENCE project (grant agreement  
576 number 805 FOE 2015).

## Appendix

**Table A1:** Field-derived TGSD together with the corresponding bi-Gaussian and bi-Weibull distributions for the Avellino Plinian. TGSDs are expressed in weight percentage (wt. %) and displayed in Fig. 6. The related grain-size class fractions are reported in Table 3. Colours are consistent with Fig. 6 and Table 3.

Diameter ( $\Phi$ )	Field TGSD	bi-Gaussian	bi-Weibull
-6	0.00	0.00	0.00
-5	0.35	0.00	0.00
-4	1.61	0.03	0.00
-3	3.31	0.49	0.26
-2	5.09	3.83	4.07
-1	7.26	14.35	15.38
0	18.00	25.72	23.69
1	27.66	22.17	20.60
2	13.53	10.31	12.46
3	6.13	6.65	7.42
4	7.33	8.29	7.98
5	6.31	5.95	5.28
6	3.07	1.91	2.04
7	0.35	0.27	0.60
8	0.00	0.02	0.16
9	0.00	0.00	0.04
10	0.00	0.00	0.01

**Table A2:** Field-derived TGSD from Macedonio et al. (2008) together with the corresponding bi-Gaussian and bi-Weibull distributions for the Pompeii Plinian eruption. TGSDs are expressed in weight percentage (wt. %) and displayed in Fig. 6. The related grain-size class fractions are reported in Table 3. Colours are consistent with Fig. 6 and Table 3.

Diameter ( $\Phi$ )	Field TGSD	bi-Gaussian	bi-Weibull
-6	0.00	0.59	0.00
-5	1.00	1.47	0.10
-4	3.98	3.13	0.80
-3	7.00	5.65	3.32
-2	6.00	8.69	7.97
-1	6.01	11.35	12.61
0	12.03	12.59	14.43
1	17.03	11.88	12.88
2	10.04	9.58	9.49
3	6.01	7.19	6.71
4	7.00	7.53	8.66
5	9.06	9.87	10.54
6	9.07	7.53	7.28
7	5.03	2.53	3.39
8	1.02	0.38	1.27
9	0.00	0.04	0.42
10	0.00	0.00	0.13

**Table A3:** Field-derived TGSD together with the corresponding bi-Gaussian and bi-Weibull distributions for the Pollena sub-Plinian eruption. TGSDs are expressed in weight percentage (wt. %) and displayed in Fig. 6. The related grain-size class fractions are reported in Table 3. Colours are consistent with Fig. 6 and Table 3.

Diameter ( $\Phi$ )	Field TGSD	bi-Gaussian	bi-Weibull
-6	0.00	1.31	0.12
-5	0.38	2.63	1.04
-4	2.08	4.56	3.95
-3	7.67	6.81	8.38
-2	9.97	8.77	11.45
-1	10.48	9.76	11.28
0	7.32	9.36	8.70
1	5.18	7.74	5.59
2	13.57	5.61	3.15
3	1.15	4.96	4.03
4	9.49	10.81	13.65
5	13.65	16.86	15.55
6	15.82	9.12	8.54
7	3.26	1.59	3.22
8	0.00	0.11	1.00
9	0.00	0.01	0.28
10	0.00	0.00	0.08

**Table A4:** Field-derived TGSD from Folch and Sulpizio (2010) together with the corresponding bi-Gaussian and bi-Weibull distributions for the Pollena sub-Plinian eruption. TGSDs are expressed in weight percentage (wt. %) and displayed in Fig. 6. The related grain-size class fractions are reported in Table 3. Colours are consistent with Fig. 6 and Table 3.

Diameter ( $\Phi$ )	Field TGSD	bi-Gaussian	bi-Weibull
-6	0.00	0.99	0.01
-5	0.00	2.00	0.20
-4	4.14	3.60	1.27
-3	5.70	5.72	4.28
-2	6.92	8.03	8.79
-1	7.76	9.99	12.35
0	10.36	11.00	12.92
1	12.31	10.76	10.78
2	10.59	9.66	8.17
3	8.14	9.18	9.28
4	10.44	10.20	11.97
5	10.33	9.86	10.09
6	7.86	6.08	5.80
7	5.10	2.22	2.60
8	0.00	0.54	1.00
9	0.00	0.13	0.36
10	0.00	0.04	0.12

**Table A5:** Field-derived TGSD together with the corresponding bi-Gaussian and bi-Weibull distributions for the 1906 Violent Strombolian eruption. TGSDs are expressed in weight percentage (wt. %) and displayed in Fig. 6. The related grain-size class fractions are reported in Table 3. Colours are consistent with Fig. 6 and Table 3.

Diameter ( $\Phi$ )	Field TGSD	bi-Gaussian	bi-Weibull
-6	0.00	0.31	0.19
-5	0.00	1.35	1.30
-4	2.90	4.11	4.42
-3	6.41	8.59	8.85
-2	9.91	12.38	11.84
-1	11.56	12.30	11.69
0	12.44	8.72	9.15
1	6.53	6.78	6.32
2	5.17	11.81	12.01
3	18.41	17.34	18.40
4	13.23	12.07	10.60
5	7.67	3.70	3.74
6	3.70	0.50	1.08
7	2.07	0.03	0.29
8	0.00	0.00	0.08
9	0.00	0.00	0.02
10	0.00	0.00	0.01

**Table A6:** Field-derived TGSD together with the corresponding bi-Gaussian and bi-Weibull distributions for the 1944 Violent Strombolian eruption. TGSDs are expressed in weight percentage (wt. %) and displayed in Fig. 6. The related grain-size class fractions are reported in Table 3. Colours are consistent with Fig. 6 and Table 3.

Diameter ( $\Phi$ )	Field TGSD	bi-Gaussian	bi-Weibull
-6	0.00	1.21	0.42
-5	1.20	4.57	3.14
-4	6.96	11.48	12.88
-3	17.20	18.00	18.68
-2	17.66	18.18	16.98
-1	15.71	13.69	14.09
0	13.36	10.00	11.37
1	8.21	7.98	8.54
2	7.54	6.18	5.85
3	3.26	4.21	3.66
4	3.29	2.46	2.12
5	4.03	1.23	1.15
6	1.57	0.53	0.59
7	0.02	0.19	0.29
8	0.00	0.06	0.14
9	0.00	0.02	0.06
10	0.00	0.00	0.03

1299  
1300  
1301  
1302  
1303  
1304  
1305  
1306  
1307  
1308  
1309  
1310  
1311  
1312  
1313  
1314  
1315  
1316  
1317  
1318  
1319  
1320  
1321  
1322  
1323  
1324  
1325  
1326  
1327  
1328  
1329  
1330  
1331  
1332  
1333  
1334  
1335  
1336  
1337  
1338  
1339  
1340  
1341  
1342  
1343  
1344  
1345  
1346  
1347  
1348  
1349  
1350  
1351  
1352  
1353  
1354  
1355  
1356  
1357

## References

1. Arrighi, S., Principe, C., and Rosi, M. Violent strombolian and sub-Plinian eruptions at Vesuvius during post-1631 activity. *Bull. Volcanol.* 63, 126–150, doi: 10.1007/s004450100130, 2001.
2. Barsotti, S., Neri, A., Bertagnini, A., Cioni, R., Mulas, M., and Mundula, F. Dynamics and tephra dispersal of Violent Strombolian eruptions at Vesuvius: insights from field data, wind reconstruction and numerical simulation of the 1906 event. *Bull. Volcanol.* 77, 58, doi: 10.1007/s00445-015-0939-6, 2015.
3. Bertagnini, A., Landi, P., Santacroce, R., and Sbrana, A. The 1906 eruption of Vesuvius: from magmatic to phreatomagmatic activity through the flashing of a shallow depth hydrothermal system. *Bull. Volcanol.*, 53, 517–532, 1991.
4. Bertagnini A., Landi P., Rosi M., and Vigliaragio A. The Pomici di Base Plinian eruption of Somma-Vesuvius. *J. Volcanol. Geotherm. Res.*, 83, 3, 219–239, 1998.
5. Bonadonna, C., and Houghton, B.F. Total grain-size distribution and volume of tephra-fall deposits. *Bull. Volcanol.* 67, 441–456, doi: 10.1007/s00445-004-0386-2, 2005.
6. Bonadonna, C., and Costa, A. Plume height, volume, and classification of explosive volcanic eruptions based on the Weibull function. *Bull. Volcanol.* 75, 742, doi: 10.1007/s00445-013-0742-1, 2013.
7. Bonadonna, C., Biass, S., and Costa, A. Physical characterization of explosive volcanic eruptions based on tephra deposits: Propagation of uncertainties and sensitivity analysis. *J. Volcanol. Geotherm. Res.* 296, 80–100, doi: 10.1016/j.jvolgeores.2015.03.009, 2015.
8. Büttner, R., Dellino, P., Raue, H., Sonder, I., and Zimanowski, B. Stress-induced brittle fragmentation of magmatic melts: Theory and experiments. *J. Geophys. Res.*, 111, B08204, doi:10.1029/2005JB003958, 2006.
9. Carey, S.N., and Sigurdsson, H. Influence of particle aggregation on deposition of distal tephra from the May 18, 1980, eruption of Mount St-Helens volcano. *J. Geophys. Res.* 87, B8, 7061–7072, doi: 10.1029/JB087iB08p07061, 1982.
10. Cioni, R., Santacroce, R., and Sbrana, A. Pyroclastic deposits as a guide for reconstructing the multi-stage evolution of the Somma-Vesuvius caldera. *Bull. Volcanol.* 60, 207–222, 1999.
11. Cioni, R., Longo, A., Macedonio, G., Santacroce, R., Sbrana, A., Sulpizio, R., and Andronico, D. Assessing pyroclastic fall hazard through field data and numerical simulations: example from Vesuvius. *J. Geophys. Res.* 108, B2, 2063. doi: 10.1029/2001JB000642, 2003a.
12. Cioni, R., Sulpizio, R., and Garruccio, N. Variability of the eruption dynamics during a Subplinian event: the Greenish Pumice eruption of Somma-Vesuvius (Italy). *J. Volcanol. Geotherm. Res.* 124, 1–2, 89–114, doi: 10.1016/S0377-0273(03)00070-2, 2003b.
13. Cioni, R., Gurioli, L., Lanza, R., and Zanella, E. Temperature of the A.D. 79 pyroclastic density current deposits (Vesuvius, Italy). *J. Geophys. Res.* 109, B02207, doi: 10.1029/2002JB002251, 2004.
14. Cioni, R., Bertagnini, A., Santacroce, R., and Andronico, D. Explosive activity and eruption scenarios at Somma-Vesuvius (Italy): towards a new classification scheme. *J. Volcanol. Geotherm. Res.* 178, 331–346, doi: 10.1016/j.jvolgeores.2008.04.024, 2008.
15. Cole, P.D., and Scarpati, C. The 1944 eruption of Vesuvius, Italy: combining contemporary accounts and field studies for a new volcanological reconstruction. *Geol. Mag.* 147, 3, 391–415, doi: 10.1017/S0016756809990495, 2010.
16. Costa, A., Folch, A., and Macedonio, G. A model for wet aggregation of ash particles in volcanic plumes and clouds: 1. Theoretical formulation. *J. Geophys. Res.* 115, B09201. doi:10.1029/2009JB007175, 2010.
17. Costa, A., Pioli, L., and Bonadonna, C. Assessing tephra total grain-size distribution: Insights from field data analysis. *Earth Planet. Sci. Lett.* 443, 90–107, doi: 10.1016/j.epsl.2016.02.040, 2016.
18. Costa, A., Pioli, L., and Bonadonna, C. Corrigendum to “Assessing tephra total grain-size distribution: Insights from field data analysis”. [*Earth and Planetary Sci. Lett.* 443, 90–107, 2016]; *Earth and Planetary Sci. Lett.* doi: 10.1016/j.epsl.2017.03.003, 2017.
19. Cubellis, E., Marturano, A., and Pappalardo, L. Le ceneri distali dell'eruzione del Vesuvio del marzo 1944 raccolte a Devoli (Albania). *Quaderni di geofisica* 113, 2013, in italian.
20. De Lorenzo, G. The eruption of Vesuvius in April 1906. *Q. J. Geol. Soc.* 62, 476–483, 1906.
21. Durant, A.J., Rose, W.I., Sarna-Wojcicki, A.M., Carey, S., and Volentik, A.C.M. Hydrometeor-enhanced tephra sedimentation: Constraints from the 18 May 1980 eruption of Mount St. Helens. *J. Geophys. Res.* 114, B03204, doi: 10.1029/2008JB005756, 2009.
22. Durant, A.J., Bonadonna, C., and Horwell, C.J. Atmospheric and Environmental Impacts of Volcanic Particulates. *Elements* 6, 235–240, doi: 10.2113/gselements.6.4.235, 2010.
23. Folch A., Cavazzoni C., Costa A., Macedonio G. An automatic procedure to forecast tephra fallout, *J. Volcanol. Geotherm. Res.*, 177, 767-777, doi:10.1016/j.jvolgeores.2008.01.046, 2008.

1358  
1359  
1360  
1361  
1362  
1363  
1364  
1365  
1366  
1367  
1368  
1369  
1370  
1371  
1372  
1373  
1374  
1375  
1376  
1377  
1378  
1379  
1380  
1381  
1382  
1383  
1384  
1385  
1386  
1387  
1388  
1389  
1390  
1391  
1392  
1393  
1394  
1395  
1396  
1397  
1398  
1399  
1400  
1401  
1402  
1403  
1404  
1405  
1406  
1407  
1408  
1409  
1410  
1411  
1412  
1413  
1414  
1415  
1416

24. Folch, A., and Sulpizio, R. Evaluating long-range volcanic ash hazard using supercomputing facilities: application to Somma-Vesuvius (Italy), and consequences for civil aviation over the Central Mediterranean Area. *Bull. Volcanol.* 72, 1039–1059, doi: 10.1007/s00445-010-0386-3, 2010.
25. Folch, A., Costa, A., Durant, A., and Macedonio, G. A model for wet aggregation of ash particles in volcanic plumes and clouds: 2. Model application. *J. Geophys. Res.* 115, B09202. doi:10.1029/2009JB007176, 2010.
26. Folch, A. A review of tephra transport and dispersal models: Evolution, current status, and future perspectives. *J. Volcanol. Geotherm. Res.* 235–236, 96–115, doi: 10.1016/j.volgeores.2012.05.020, 2012.
27. Folch, A., Costa, A., and Basart, S. Validation of the FALL3D ash dispersion model using observations of the 2010 Eyjafjallajökull volcanic ash clouds. *Atmos. Env.* 48, 165–183. doi:10.1016/j.atmosenv.2011.06.072, 2012.
28. Gouhier, M., Eychenne, J., Azzaoui, N., Guillin, A., Deslandes, M., Poret, M., Costa, A., and Husson, P. Low efficiency of large volcanic eruptions in transporting very fine ash into the atmosphere. *Nature Sci. Rep.*, 9, 1449, doi:10.1038/s41598-019-38595-7, 2019.
29. Guffanti, M., Ewert, J.W., Gallina, G.M., Bluth, G.J.S., and Swanson, G.L. Volcanic-ash hazard to aviation during the 2003-2004 eruption activity of Anatahan volcano Commonwealth of the Northern Mariana Islands. *J. Volcanol. Geotherm. Res.* 146, 241–255, doi:10.1016/j.volgeores.2004.12.011, 2005.
30. Gurioli, L., Sulpizio, R., Cioni, R., Sbrana, A., Santacroce, R., Luperini, W., and Andronico, D. Pyroclastic flow hazard assessment at Somma-Vesuvius based on the geological record. *Bull. Volcanol.*, 72, 1021-1038, doi:10.1007/s00445-010-0379-2, 2010.
31. Hobbs, W.H. The grand eruption of Vesuvius in 1906. *J Geol* 14–7, 636–655, 1906.
32. Imbò, G. L'attività eruttiva e relative osservazioni nel corso dell'intervallo inter-eruttivo 1906–1944 ed in particolare del parossismo del Marzo 1944. *Annali Osservatorio Vesuviano*, V serie, volume unico, 185– 380, 1949, in italian.
33. Jones, T.J., and Russel, J.K. Ash production by attrition in volcanic conduits and plumes. *Nature Sci. Rep.*, 7, 5538, doi:10.1038/s41598-017-05450-6, 2017.
34. Kaminski, E., and Jaupart, C. The size distribution of pyroclasts and the fragmentation sequence in explosive volcanic eruptions. *J. Geophys. Res.* 103, B12, 29759–29779, doi: 10.1029/98JB02795, 1998.
35. Krumbein, W.C. Size Frequency Distribution of Sediments. *J. Sediment. Res.* 4, 2, 65-77, doi: 10.1306/D4268EB9-2B26-11D7-8648000102C1865D, 1934.
36. Macedonio, G., Pareschi, M.T., and Santacroce R. A numerical Simulation of Plinian Fall Phase of 79 A.D. Eruption of Vesuvius. *J. Geophys. Res.* 93, B12, 14817–14827, doi: 10.1029/JB093iB12p14817, 1988.
37. Macedonio, G., Costa, A., and Folch, A. Ash fallout scenarios at Vesuvius: Numerical simulations and implications for hazard assessment. *J. Volcanol. Geotherm. Res.* 178, 3, 366–377, doi: 10.1016/j.jvolgeores.2008.08.014, 2008.
38. Marzocchi, W., Sandri, L., Gasperini, P., Newhall, C., and Boschi E. Quantifying probabilities of volcanic events: The example of volcanic hazard at Mount Vesuvius. *J. Geophys. Res.* 109, B11201, doi:10.1029/2004JB003155, 2004.
39. Massaro, S., Costa, A., and Sulpizio, R. Evolution of the magma feeding system during a Plinian eruption: The case of Pomici di Avellino eruption of Somma-Vesuvius, Italy. *Earth Planetary Sci. Lett.*, 482, 545–555, doi:10.1016/j.epsl.2017.11.030, 2018.
40. Mastin, L.G., Van Eaton, A.R., and Durant, A.J. Adjusting particle-size distributions to account for aggregation in tephra-deposit model forecasts. *Atmos. Chem. Phys.* 16, 9399–9420, doi: 10.5194/acp-16-9399-2016, 2016.
41. Mele, D., Sulpizio, R., Dellino, P., and La Volpe, L. Stratigraphy and eruptive dynamics of a pulsating Plinian eruption of Somma-Vesuvius: the Pomici di Mercato (8900 years B.P.). *Bull. Volcanol.*, 73, 257–278, doi:10.1007/s00445-010-0407-2, 2011.
42. Mueller, S.B., Kueppers, U., Ametsbichler, J., Cimarelli, C., Merrison, J.P., Poret, M., Wadsworth, F.B., and Dingwell, D.B. Stability of volcanic ash aggregates and break-up processes. *Nature – Sci. Rep.* 7, 7440. doi: 10.1038/s41598-017-07927-w, 2017.
43. Mueller, S.B., Houghton, B.F., Swanson, D.A., Fagents, S.A., Klawonn, M., and Poret, M. Total grain-size distribution of a Hawaiian tephra deposit: case study of the 1959 Kīlauea Iki eruption Hawai'i. *Bull. Volcanol.*, xxx, xx–xx, doi:xxxxxxx, 2019.
44. Murrow, P.J., Rose, W.I., and Self, S. Determination of the total grain size distribution in a Vulcanian eruption column, and its implications to stratospheric aerosol perturbation. *Geophys. Res. Lett.* 7, 11, 893–896, doi: 10.1029/GL007i011p00893, 1980.
45. Neri, A., Aspinall, W.P., Cioni, R., Bertagnini, A., Baxter, P.J., Zuccaro, G., Andronico, D., Barsotti, S., Cole, P.D., Esposito Ongaro, T., Hincks, T.K., Macedonio, G., Papale, P., Rosi, M., Santacroce, R., and Woo, G. Developing an Event Tree for pyroclastic hazard and risk assessment at Vesuvius. *J. Volcanol. Geotherm. Res.*, 178, 397-415, doi:10.1016/j.jvolgeores.2008.05.014, 2008.
46. Pedrazzi, D., Suñe-Puchol, I., Aguirre-Díaz, G., Costa, A., Smith, V.C., Poret, M., Dávila-Harris, P., Miggins, D.P., Hernández, W., and Gutiérrez, E. The Ilopango Tierra Blanca Joven (TBJ) eruption, El Salvador: Volcano-stratigraphy

- 1417  
1418  
1419706 and physical characterization of the major Holocene event of Central America. *J. Volcanol. Geotherm. Res.*, 377, 81–102,  
1420707 doi:10.1016/j.jvolgeores.2019.03.006, 2019.
- 1421708 47. Perret F.A. The Vesuvius eruption of 1906. Study of a volcanic cycle. *Carnegie Inst Washington Pub* 339, pp 151, 1924.  
1422709 48. Pesce, A., and Rolandi, G. Vesuvio 1944. L'ultima eruzione, Napoli, *Edizioni Magma*, p. 216, 2000.  
1423710 49. Poret, M., Costa, A., Folch, A., and Marti, A. Modelling tephra dispersal and ash aggregation: The 26th April 1979  
1424711 eruption, La Soufrière St. Vincent. *J. Volcanol. Geotherm. Res.* 347, 207–220, doi: 10.1016/j.jvolgeores.2017.09.012,  
1425712 2017.  
1426713 50. Poret, M., Corradini, S., Merucci, L., Costa, A., Andronico, D., Vulpiani, G., Montopoli, M., and Freret-Lorgeril, V.  
1427714 Reconstructing volcanic plume evolution integrating satellite and ground-based data: application to the 23 November  
1428715 2013 Etna eruption. *Atmos. Chem. Phys.* 18, 7, 4695–4714, doi: 10.5194/acp-18-4695-2018, 2018a.  
1429716 51. Poret, M., Costa, A., Andronico, D., Scollo, S., Gouhier, M., and Cristaldi, A. Modelling eruption source parameters by  
1430717 integrating field, ground-based and satellite-based measurements: The case of the 23 February 2013 Etna paroxysm. *J.*  
1431718 *Geophys. Res.: Solid Earth* 123, doi: 10.1029/2017JB015163, 2018b.  
1432719 52. Poret, M. Modelling ash cloud dispersion and the impact of ash aggregation during volcanic eruptions. Thesis, University  
1433720 of Bologna (Italy) *Alma Matter Studiorum*, May 2018, doi:10.13140/RG.2.2.35832.55041, 2018c.  
1434721 53. Poret, M., Finizola, A., Ricci, T., Ricciardi, G.P., Linde, N., Mauri, G., Barde-Cabusson, S., Guichet, X., Baron, L.,  
1435722 Shakas, A., Gouhier, M., Levieux, G., Morin, J., Roulleau, E., Sortino, F., Vasallo, R., Di Vito, M.A., and Orsi, G. The  
1436723 buried boundary of Vesuvius 1631 caldera revealed by present-day diffuse degassing. *J. Volcanol. Geotherm. Res.* 375,  
1437724 43–56, doi:10.1016/j.jvolgeores.2019.01.029, 2019.
- 1438725 54. Rolandi, G., Bellucci, F., and Cortini, M. A new model for the formation of the Somma Caldera. *Mineral. Petro.* 80, 27–  
1439726 44, doi: 10.1007/s00710-003-0018-0, 2004.
- 1440727 55. Rose, W.I., and Durant, A.J. Fine ash content of explosive eruptions. *J. Volcanol. Geotherm. Res.* 186, 1–2, 32–39, doi:  
1441728 10.1016/j.jvolgeores.2009.01.010, 2009.
- 1442729 56. Rust, A.C., and Cashman, K.V. Permeability controls on expansion and size distributions of pyroclasts. *J. Geophys.*  
1443730 *Res.* 116, B11202, doi: 10.1029/2011JB008494, 2011.
- 1444731 57. Sabatini, V. L'eruzione vesuviana dell'Aprile 1906. *Boll. Del R. Comitato geologico d'Italia*, 3, 169–229, 1906, in Italian.  
1445732 58. Santacroce, R. Somma-Vesuvius. *Quaderni. Ric. Sci.* 114, pp 230, Cons. Naz. delle Ric., Rome, 1987.  
1446733 59. Santacroce, R., and Sbrana, A. Geological map of Vesuvius at the scale 1:15,000. SELCA editore, Firenze, 2003.  
1448734 60. Santacroce, R., Cioni, R., Marianelli, P., Sbrana, A., Sulpizio, R., Zanchetta, G., Donahue, D.J., and Joron, J.L. Age and  
1449735 whole rock-glass compositions of proximal pyroclastics from the major explosive eruptions of Somma-Vesuvius: a review  
1450736 as a tool for distal tephrostratigraphy. *J. Volcanol. Geotherm. Res.* 177, 1–18. doi: 10.1016/j.jvolgeores.2008.06.009,  
1451737 2008.
- 1452738 61. Scandone, R., Iannone, F., and Mastrolorenzo, G. Stima dei parametri dinamici dell'eruzione del 1944 del Vesuvio. *Boll.*  
1453739 *GNV* 2, 487–512, 1986.
- 1454740 62. Scandone, R., Giacomelli, L., and Gasparini, P. Mount Vesuvius: 2000 yrs of volcanological observations. *J. Volcanol.*  
1455741 *Geotherm. Res.*, 58, 263–271, 1993.
- 1456742 63. Scollo, S., Folch, A., and Costa, A. A parametric and comparative study of different tephra fallout models. *J. Volcanol.*  
1457743 *Geotherm. Res.* 176, 2, 199–211, doi: 10.1016/j.jvolgeores.2008.04.002, 2008.
- 1458744 64. Scollo, S., Prestifilippo, M., Pecora, E., Corradini, S., Merucci, L., Spata, G., and Coltelli, M. Eruption column height  
1459745 estimation of the 2011–2013 Etna lava fountains. *Annals Geophys.* 57, 2, S0214, doi: 10.4401/ag-6396, 2014.
- 1460746 65. Sevink, J., Van Bergen, M.J., Van der Plicht, J., Feiken, H., Anastasia, C., and Huizinga, A. Robust date for the Bronze  
1461747 Age Avellino eruption (Somma-Vesuvius): 3945 ± 10 cal BP (1995 ± 10 cal BC). *Quat. Sci. Rev.*, 30, 1035–1046, 2011.
- 1462748 66. Sigurdsson, H., Carey, S., Cornell, W., and Pescatore, T. The eruption of Vesuvius A.D. 79. *Nat. Geo. Res.*, 1, 3, 332–387,  
1463749 1985.
- 1464750 67. Spanu, A., De Vitturi, M.M., and Barsotti, S. Reconstructing eruptive source parameters from tephra deposit: A numerical  
1465751 study of medium-sized explosive eruptions at Etna volcano. *Bull. Volcanol.* 78, 9, 59, doi: 10.1007/s00445-016-1051-2,  
1466752 2016.
- 1467753 68. Sulpizio, R., Mele, D., Dellino, P., and La Volpe, L. A complex, Subplinian-type eruption from low-viscosity, phonolitic  
1468754 to tephriphonolitic magma: the AD 472 (Pollena) eruption of Somma- Vesuvius, Italy. *Bull. Volcanol.* 67, 743–767, doi:  
1469755 10.1007/s00445-005-0414-x, 2005.
- 1470756 69. Sulpizio, R., Mele, D., Dellino, P., and La Volpe, L. Deposits and physical properties of pyroclastic density currents  
1471757 during complex Subplinian eruptions: the AD 472 (Pollena) eruption of Somma-Vesuvius, Italy. *Sedimentology* 54, 3,  
1472758 607–635, doi: 10.1111/j.1365-3091.2006.00852.x, 2007.

1476  
1477  
1478  
1479  
1480  
1481  
1482  
1483  
1484  
1485  
1486  
1487  
1488  
1489  
1490  
1491  
1492  
1493  
1494  
1495  
1496  
1497  
1498  
1499  
1500  
1501  
1502  
1503  
1504  
1505  
1506  
1507  
1508  
1509  
1510  
1511  
1512  
1513  
1514  
1515  
1516  
1517  
1518  
1519  
1520  
1521  
1522  
1523  
1524  
1525  
1526  
1527  
1528  
1529  
1530  
1531  
1532  
1533  
1534

70. Sulpizio, R., Caron, B., Giaccio, B., Paternò, M., Siani, G., Zanchetta, G., and Santacroce, R. The dispersal of ash during explosive eruptions from central volcanoes and calderas: an underestimated hazard for the Central Mediterranean area. *IOP Publishing, Collapse Calderas Workshop, Series 3*, doi: 10.1088/1755-1307/3/1/012031, 2008.
71. Sulpizio, R., Van Welden, A., Caron, B., and Zanchetta, G. The Holocene tephrostratigraphic record of Lake Shkodra (Albania and Montenegro). *J. Quat. Sci.* 25, 5, 633–650, doi:10.1002/jqs.1334, 2010a.
72. Sulpizio, R., Cioni, R., Di Vito, M.A., Mele, D., Bonasia, R., and Dellino, P. The Pomici di Avellino eruption of Somma-Vesuvius (3.9 ka BP) part I: stratigraphy, compositional variability and eruptive dynamics. *Bull. Volcanol.* 72, 539–558, doi:10.1007/s00445-009-0339-x, 2010b.
73. Sulpizio, R., Bonasia, R., Dellino, P., Mele, D., Di Vito, M.A., and La Volpe, L. The Pomici di Avellino eruption of Somma-Vesuvius (3.9 ka BP) part II: sedimentology and physical volcanology of pyroclastic density current deposits. *Bull. Volcanol.* 72: 559–577, doi:10.1007/s00445-009-0340-4, 2010c.
74. Sulpizio, R., Zanchetta, G., D’Orazio, M., Vogel, H., and Wagner, B. Tephrostratigraphy and tephrochronology of lakes Ohrid and Prespa, Balkans. *Biogeosciences* 7, 3273–3288, doi: 10.5194/bg-7-3273-2010, 2010d.
75. Sulpizio, R., Folch, A., Costa, A., Scaini, C., and Dellino, P. Hazard assessment of far-range volcanic ash dispersal from a violent Strombolian eruption at Somma-Vesuvius volcano, Naples, Italy: implications on civil aviation. *Bull. Volcanol.* 74, 2205–2218, doi: 10.1007/s00445-012-0656-3, 2012.
76. Sulpizio, R., Zanchetta, G., Caron, B., Dellino, P., Mele, D., Giaccio, B., Insinga, D., Paternò, M., Siani, G., Costa, A., Macedonio, G., and Santacroce, R. Volcanic ash hazard in the Central Mediterranean assessed from geological data. *Bull. Volcanol.* 76, 866, doi: 10.1007/s00445-014-0866-y, 2014.
77. Tomašek, I., Horwell, C.J., Damby, D.E., Barošová, H., Geers, C., Petri-Fink, A., Rothen-Rutishauser, B., and Clift, M.J.D. Combined exposure of diesel exhaust particles and respirable Soufrière Hills volcanic ash causes a (pro-)inflammatory response in an in vitro multicellular epithelial tissue barrier model. *Particle and Fibre Toxicology* 13, 1, 67, doi: 10.1186/s12989-016-0178-9, 2016.
78. Tomašek, I., Horwell, C.J., Bisig, C., Damby, D.E., Comte, P., Czerwinski, J., Petri-Fink, A., Clift, M.J.D., Drasler, B., and Rothen-Rutishauser, B. Respiratory hazard assessment of combined exposure to complete gasoline exhaust and respirable volcanic ash in a multicellular human lung model at the air-liquid interface. *Env. Pollution* 238, 977–987, doi: 10.1016/j.envpol.2018.01.115, 2018.
79. Vogel, H., Zanchetta, G., Sulpizio, R., Wagner, B., and Nowaczyk, N. A tephrostratigraphic record for the last glacial–interglacial cycle from Lake Ohrid, Albania and Macedonia. *J. Quat. Sci.* 25, 3, 320–338, doi: 10.1002/jqs.1311, 2009.
80. Volentik, A.C.M., Bonadonna, C., Connor, C.B., Connor, L.J., and Rosi, M. Modeling tephra dispersal in absence of wind: Insights from the climactic phase of the 2450 BP Plinian eruption of Pululagua volcano (Ecuador). *J. Volcanol. Geotherm. Res.*, 193 (1–2), 117–136, 2010.
81. Walker, G.P.L., 1981. The Waimihia and Hatepe plinian deposits from the rhyolitic Taupo Volcanic Centre. *New Zealand J. Geol. Geophys.* 24, 3, 305–324, 1981.
82. Watt, S.F.L., Gilbert, J.S., Folch, A., and Phillips, J.C. An example of enhanced tephra deposition driven by topographic induced atmospheric turbulence. *Bull. Volcanol.* 77, 35, doi: 10.1007/s00445-015-0927-x, 2015.